Weak impositions of Dirichlet boundary conditions in solid mechanics: a critique of current approaches and extension to partially prescribed boundaries

Kaizhou Lu[a,b], Charles E. Augarde[b], William M. Coombs[b], Zhendong Hu[a,*]

[a]*School of Aerospace Engineering and Applied Mechanics, Tongji University, Shanghai, 200092, P.R.C*
[b]*Department of Engineering, Durham University, Durham, DH1 3LE, UK*

Abstract

In this article we first review various approaches developed to date for the weak imposition of Dirichlet boundary conditions in fictitious domain analysis for elasticity problems. The Hellinger-Reissner (H-R) principle, the linked Lagrange multiplier (LLM) method, the implicit boundary method and the fat boundary method are discussed along with the well-known Lagrange multiplier, penalty and Nitsche's methods. We state these approaches in a common form starting with energy functionals and weak forms, and discretise using the fictitious domain finite element method. Previous formulations of these methods were in general developed for full prescription along the Dirichlet boundary, which generally implies no local effect of boundary inclination. However, partially prescribed conditions (such as the structural roller boundary condition) with inclination have wide practical applications in engineering. Here we provide techniques of imposing such boundary conditions in these methods in detail. For those methods that contain algorithmic parameters, such as the penalty and Nitsche's methods, extra computation or empirical estimation is necessary to decide values of the parameters, and hence we discuss parametric and convergence behaviours through numerical examples to provide guidance on the choice of parameters.

Keywords: Dirichlet boundary conditions, fictitious domain, immersed boundary, Lagrange multipliers, Nitsche's method, implicit boundary method

1. Introduction

1.1. Fictitious domain methods

In the classical finite element method, discretisation of the problem domain into a finite element mesh that matches the geometric boundary is required. Mesh generation then becomes a non-trivial process especially for structures with complex geometry, often resulting in distorted or ill-conditioned elements. Apart from meshfree methods, an alternative approach to circumvent the time-consuming mesh generation procedure is to use a mesh that does not conform to the physical domain. An early suggestion by Peskin [1] to embed the domain of interest into an extended fictitious domain was proposed in 1972 in a numerical simulation of flow patterns around heart

*Corresponding author.
Email address: zdhu@tongji.edu.cn (Zhendong Hu)

valves, a method which became known as the immersed boundary method [2], also as the fictitious domain method [3], the embedded boundary method [4], the non-conforming mesh method [5] and the non-matching mesh method [6] (of note is that the terms "non-conforming" and "non-matching" are more often used for several detached sub-meshes in a decomposed domain [7, 8]).

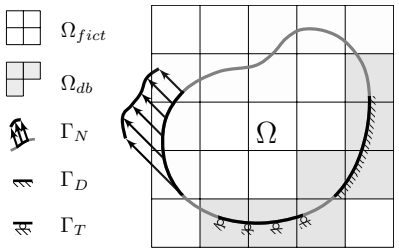

Figure 1: Domain setting of the model problem with boundary conditions.

Fictitious domain approaches embed the domain of interest Ω into an extended computational domain Ω_{fict} with a much simpler geometry, such that the problem can be discretised using a structured mesh. For instance, the fictitious domain can be a simple rectangle and easily meshed using finite elements aligned with Cartesian coordinates (Figure 1). As the problem domain is enlarged, integrals over the domain of interest should still be evaluated within the physical domain, such that an appropriate strategy of numerical integration is necessary for elements cut by the boundary. The integration strategy adopted in this article is discussed in Section 2.2.

1.2. Weak imposition of Dirichlet boundary conditions and problem statement

The major difficulty of the fictitious domain setting comes from incorporating Dirichlet boundary conditions. As the nodes are not guaranteed to coincide with the geometric boundary in the mesh, the traditional way to impose Dirichlet boundary conditions in the finite element method directly is not feasible. There are approaches, such as point collocation that impose boundary conditions strongly, however, major effort has been expended on weak imposition methods which include Dirichlet boundary conditions during method formulation.

This article present formulations based on the fictitious domain finite element method in the two-dimensional case for simplicity. However, the methods are easily extensible to meshfree or other fictitious domain approaches, and to the three-dimensional case. Linear elasticity is considered here as the model problem with the physical domain $\Omega \in \mathscr{R}^2$, and three boundary conditions are described for the physical domain so that $\partial\Omega = \Gamma_D \cup \Gamma_N \cup \Gamma_T$, as shown in Figure 1. Ω_{db} in the figure represents elements cut by $\Gamma_D \cup \Gamma_T$, and we further denote that $\Omega_\Gamma = \Omega \cap \Omega_{db}$. Γ_D and Γ_N respectively denote Dirichlet and Neumann boundaries. Γ_T denotes partially prescribed boundaries, where both Dirichlet and Neumann boundary conditions are applied, but in two orthogonal directions described by local coordinates $x_i'(i = 1, 2)$. Specifically, we designate x_1' and x_2' as the directions where Dirichlet and Neumann boundary conditions are respectively imposed. So-called roller boundary conditions, which have prescribed displacement in the normal direction and Neumann boundary conditions tangentially, are typical conditions for Γ_T. The strong form of the problem is stated as

$$\begin{array}{llll} -\nabla\cdot\boldsymbol{\sigma} = \boldsymbol{b} & \text{in } \Omega, & \boldsymbol{u} = \bar{\boldsymbol{u}} & \text{on } \Gamma_D, \qquad \boldsymbol{\sigma}\cdot\boldsymbol{n} = \bar{\boldsymbol{g}} \quad \text{on } \Gamma_N, \\ \alpha_{1j}u_j = \bar{u}_1' & \text{on } \Gamma_T, & \text{and} & \alpha_{2j}\sigma_{jk}n_k = \bar{g}_2' \quad \text{on } \Gamma_T, \end{array} \tag{1}$$

where $\boldsymbol{u}$ is the displacement vector, $\boldsymbol{\sigma}$ is the stress tensor, $\boldsymbol{b}$ is the body force vector, and $\boldsymbol{n}$ denotes the outward normal unit vector on $\partial\Omega$. $\bar{\boldsymbol{u}}$ and $\bar{\boldsymbol{g}}$ are boundary value functions on Γ_D and Γ_N, respectively; $\bar{u}_1'$ and $\bar{g}_2'$ are boundary value functions on Γ_T in respective directions. The equations are closed with the compatibility equation $\boldsymbol{\varepsilon} = \frac{1}{2}[\nabla\boldsymbol{u} + (\nabla\boldsymbol{u})^T]$ and the constitutive relation $\boldsymbol{\sigma} = \boldsymbol{E} : \boldsymbol{\varepsilon}$, where $\boldsymbol{E}$ is the elastic tensor. Dashes $(\cdot)'$ indicate quantities in local coordinates x_i' and $\boldsymbol{\alpha}$ is a second order transformation tensor where $\alpha_{ij} = \cos(x_i', x_j)$ are direction cosines. For simplicity, we denote that $\Gamma_T = \Gamma_D$ and $\Gamma_T = \Gamma_N$ for integrals only including quantities defined in the x_1' and x_2' directions respectively.

The weak imposition methods of Dirichlet boundary conditions developed so far can be classified in three groups. The first type introduces additional terms to the energy functional and the weak form to impose Dirichlet boundary conditions, and includes the Lagrange multiplier method [9], the penalty method [10], Nitsche's method [11] and the linked Lagrange multiplier (LLM) method [12]. The Hellinger-Reissner (H-R) principle [13] also fits in this group as it fulfils the Dirichlet boundary condition in its two-field energy functional. The second type of approach is known as the implicit boundary method [5] which incorporates implicit functions that satisfy the Dirichlet boundary conditions to weight the unknown field. The fat boundary method [14] fits in the last group, the main idea of which is to split the original problem into sub-problems and solve them iteratively.

Fernández-Méndez et al. [15] reviewed both weak forms and finite element formulations of the well understood Lagrange multiplier, penalty and Nitsche's methods, implemented and compared them with the continuous blending method (which has finite element discretisation near the Dirichlet boundary) and coupled it with a meshfree method in the domain. They showed results with several different choices of interpolation spaces in the Lagrange multiplier method and several different penalty values in penalty and Nitsche's methods. Zhang et al. [16] summarised energy functionals, interpolation forms and linear systems for different kinds of implicit boundary methods in a brief survey, besides the three methods mentioned above. Ramos et al. [6] surveyed different variants of the original Lagrange multiplier method which aim to overcome the stabilisation problem to be discussed later. Stenberg [17] reviewed theorems in the stability analysis of the original and stabilised Lagrange multiplier methods, and Nitsche's method, and built connections between them. Arnold et al. [18] provided an overview of the penalty method, Nitsche's method and the discontinuous Galerkin methods based on Nitsche's method. Baiges et al. [12] made a comparison between the LLM method, which they proposed in the same article, with Nitsche's formulation, rearranging the system of equations in the LLM method into a form that resembles Nitsche's method.

However, several advantageous methods were either overlooked or not discussed from their starting points in these articles. Partially prescribed boundary conditions, which play an important role in real engineering applications, are barely discussed in the literature, nor is the implementation of non-uniform Dirichlet boundary conditions. The aim of this article is to review the most significant methods for the weak imposition of Dirichlet boundary conditions developed to date, as well as link the parametric behaviour of some methods with convergence theories, which provides guidance on the choice of algorithmic parameters in these methods.

1.3. Fictitious domain methods covering Dirichlet boundary conditions

In this section, we review some recently developed fictitious domain finite element methods with novel features and closely related to the weak imposition of Dirichlet boundary conditions.

Finite cell method. The finite cell method was first proposed by Parvizian, et al. [19] as a fictitious domain finite element approach, the distinguishing feature of which is the combination of the fictitious mesh and p-version finite elements with an adaptive integration strategy. To increase the accuracy of Gauss quadrature performed over the elements cut by the boundary, hierarchical refinement techniques, such as quadtree refinement, are used to decompose the elements into sub-cells for the purpose of integration.

Another feature of the finite cell method is the weak imposition of Dirichlet boundary conditions, due to the fictitious domain setting. Different imposition methods to be introduced later in this article have been applied to the finite cell method.

WEB-method. The WEB (weighted extended B-spline) method is a finite element approach developed by Höllig et al. [20] that uses weighted multivariate B-splines as basis functions to interpolate the unknown field. The B-splines are defined on a tensor product grid, such that a non-fitting Cartesian mesh is formed in the WEB-method. To overcome the obvious difficulty of incorporating Dirichlet boundary conditions, the WEB-method employs the approach developed by Kantorovich and Krylov [21] which weights the approximation of the unknown field by an implicit function that vanishes on the Dirichlet boundary.

This approach later inspired the step function method [5] through the use of an approximate step function as the weight function. A special scheme for integration was developed, and the weighted unknown field leads to a final solution system that contains a penalty parameter and resembles the penalty method in terms of its parametric behaviour. Details of methods that use implicit functions to impose Dirichlet boundary conditions are discussed in Section 3.2.

Fat boundary method. The fat boundary method, a fictitious domain approach first introduced by [14] in 2001, really belongs to domain decomposition methods. While classical numerical methods approximate partial differential equations with a single fitted mesh, domain decomposition methods split up the original problem into several sub-problems. The main idea is to derive fast and reliable methods to solve the problem with multi-domains iteratively, which fits easily in a parallel computing environment.

The fat boundary method was developed to approximate partial differential equations in a domain with constrained holes. The initial domain of computation is split into sub-domains with dependent finite element meshes: one in the whole fictitious domain with a structured mesh and others near the holes with local meshes, such that the geometric boundaries of the holes are immersed in the background mesh of the fictitious domain. The fat boundary method incorporates Dirichlet boundary conditions in a weak sense, discussed in detail in Section 3.3.

2. Weak form and the finite element discretisation

2.1. Classical finite element formulation

We first introduce the following functional space

$$\mathscr{H}^1_{\Gamma_D}(\Omega) = \{v_i \in \mathscr{H}^1(\Omega) | \boldsymbol{v} = \bar{\boldsymbol{u}} \text{ on } \Gamma_D\} \tag{2}$$

The solution to Problem (1) is equivalent to minimising the potential energy functional stated below: find $u_i \in \mathscr{H}^1_{\Gamma_D}(\Omega)$ such that

$$\boldsymbol{u} = \arg\ \min\ \Pi(\boldsymbol{v}), \tag{3}$$

where

$$\Pi(\boldsymbol{v}) = \int_\Omega v_\varepsilon(\boldsymbol{v}) d\Omega - \int_\Omega \boldsymbol{v} \cdot \boldsymbol{b} d\Omega - \int_{\Gamma_N} \boldsymbol{v} \cdot \bar{\boldsymbol{g}} d\Gamma, \tag{4}$$

for $\forall v_i \in \mathscr{H}^1_{\Gamma_D}(\Omega)$, where the strain energy density $v_\varepsilon(\boldsymbol{v}) = \frac{1}{2}\boldsymbol{\varepsilon}(\boldsymbol{v}) : \boldsymbol{\sigma}(\boldsymbol{v})$ in linear elasticity. With $\delta(\cdot)$ denoting variation, the associated weak form statement is: find $u_i \in \mathscr{H}^1_{\Gamma_D}(\Omega)$ such that

$$\int_\Omega \boldsymbol{\varepsilon}(\delta\boldsymbol{u}) : \boldsymbol{\sigma}(\boldsymbol{u}) d\Omega = \int_\Omega \delta\boldsymbol{u} \cdot \boldsymbol{b} d\Omega + \int_{\Gamma_N} \delta\boldsymbol{u} \cdot \bar{\boldsymbol{g}} d\Gamma. \tag{5}$$

Here and in the succeeding text, the discretisation is given as

$$\boldsymbol{u}(\boldsymbol{x}) = \sum_{j=1}^{n_d} \boldsymbol{N}_j(\boldsymbol{x}) \boldsymbol{u}_j^e = \boldsymbol{N}(\boldsymbol{x}) \boldsymbol{u}^e, \tag{6}$$

where n_d is the number of element nodes, $\boldsymbol{N}_j = N_j \boldsymbol{I}_{2\times 2}$ is the product of the jth shape function and the 2×2 identity matrix, and $\boldsymbol{u}_j^e = [u, v]^T$ represent nodal unknowns of the displacement. The Voigt notation vectors of the strain and the stress are expressed as

$$\boldsymbol{\varepsilon}(\boldsymbol{u}) = [\varepsilon_x, \varepsilon_y, \gamma_{xy}]^T = \boldsymbol{B}\boldsymbol{u}^e \qquad \text{and} \qquad \boldsymbol{\sigma}(\boldsymbol{u}) = [\sigma_x, \sigma_y, \tau_{xy}]^T = \boldsymbol{D}\boldsymbol{B}\boldsymbol{u}^e, \tag{7}$$

where $\boldsymbol{D}$ denotes the elastic matrix and $\boldsymbol{B} = \mathcal{L}(\boldsymbol{N})$ with the operator being

$$\mathcal{L} = \begin{bmatrix} \partial/\partial x & 0 \\ 0 & \partial/\partial y \\ \partial/\partial y & \partial/\partial x \end{bmatrix}.$$

The resulting system of equations at element level is

$$\boldsymbol{K}\boldsymbol{u}^e = \boldsymbol{f}, \tag{8}$$

where

$$\boldsymbol{K} = \int_{\Omega^e} \boldsymbol{B}^T \boldsymbol{D} \boldsymbol{B} d\Omega \qquad \text{and} \qquad \boldsymbol{f} = \int_{\Omega^e} \boldsymbol{N}^T \boldsymbol{b} d\Omega + \int_{\Gamma_N^e} \boldsymbol{N}^T \bar{\boldsymbol{g}} d\Gamma, \tag{9}$$

with the superscript $(\cdot)^e$ denoting the regions or lines within an element. The preceding system of the classical finite element framework is derived under the assumption that $v_i \in \mathscr{H}^1_{\Gamma_D}(\Omega)$ and problems arise when it comes to fictitious domain approaches, where $v_i \in \mathscr{H}^1(\Omega)$, as there is nowhere to strongly enforce Dirichlet boundary conditions if they do not align with boundaries of the physical domain.

2.2. Numerical implementation for the fictitious domain

In this article, we focus on the imposition methods of Dirichlet boundary conditions, and a straightforward way to treat elements cut by a geometric boundary is used, shown in Figure 2; other techniques such as hierarchical refinement [22] for the cut elements are also feasible strategies. Here, a background grid that contains the physical domain is first generated, and points where the boundary and the grid intersect are captured to approximate the boundary by piecewise linear segments $\partial\Omega_h$ spanned on these intersections, with two Gauss points, marked with stars in the figure, being placed on each segment for boundary integrals.

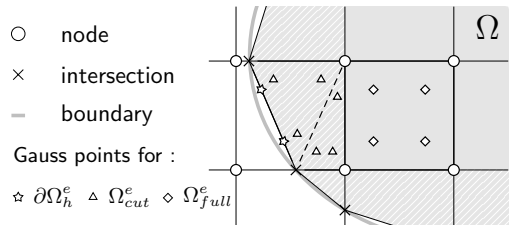

Figure 2: Approximation of the geometric boundary and integration schemes for integrals along the boundary and over the physical domain.

The integration scheme for domain integrals over Ω^e_{full} (elements that lie entirely in the physical domain) remains the same as for classical finite elements: first order Gauss quadrature is used for linear elements. As integrals over elements cut by the boundary should be evaluated within the physical domain, the physical domain of a cut element, Ω^e_{cut}, is sub-triangulated for the purposes of integration, while the element itself remains intact. Gauss locations for triangular elements are used in each triangle patch, as shown in the figure with triangular markers for linear elements.

3. Methods for weak imposition of Dirichlet boundary conditions

In this section, we present formulations of methods without considering inclined conditions on Γ_T as described in (1). The implementation of the inclined and partly prescribed conditions on Γ_T is introduced in Section 4.

3.1. Methods based on the modification of the energy functional

3.1.1. Lagrange multiplier method

The theory of introducing the Lagrange multiplier method in the finite element method to fulfil Dirichlet boundary conditions was first derived by Babuška [9]. The Lagrange multiplier method is also employed to impose Dirichlet boundary conditions in meshfree Galerkin methods [23, 24] and fictitious domain finite element methods [25].

When the geometrically admissible displacements do not satisfy Dirichlet boundary conditions in advance, i.e. $v_i \in \mathscr{H}^1(\Omega)$, Dirichlet boundary conditions can be enforced by introducing Lagrange multipliers $\boldsymbol{\gamma}$ to the energy functional (4), which becomes

$$\Pi_L(\boldsymbol{v}, \boldsymbol{\gamma}) = \Pi(\boldsymbol{v}) + \int_{\Gamma_D} \boldsymbol{\gamma} \cdot (\boldsymbol{v} - \bar{\boldsymbol{u}}) d\Gamma \tag{10}$$

and

$$(\boldsymbol{u}, \boldsymbol{\lambda}) = \arg \min_{v_i \in \mathscr{H}^1(\Omega)} \max_{\gamma_i \in \mathscr{H}^{-1/2}(\Gamma_D)} \Pi_L(\boldsymbol{v}, \boldsymbol{\gamma}). \tag{11}$$

The resulting problem is a saddle point problem, as the quadratic form of the new functional above is not positive definite. Solving the saddle point problem leads to the following weak form statement: find $u_i \in \mathscr{H}^1(\Omega)$ and $\lambda_i \in \mathscr{H}^{-1/2}(\Gamma_D)$ such that

$$\int_\Omega \boldsymbol{\varepsilon}(\delta \boldsymbol{u}) : \boldsymbol{\sigma}(\boldsymbol{u}) d\Omega - \int_\Omega \delta \boldsymbol{u} \cdot \boldsymbol{b} d\Omega - \int_{\Gamma_N} \delta \boldsymbol{u} \cdot \bar{\boldsymbol{g}} d\Gamma + \int_{\Gamma_D} \delta \boldsymbol{u} \cdot \boldsymbol{\lambda} d\Gamma + \int_{\Gamma_D} \delta \boldsymbol{\lambda} \cdot (\boldsymbol{u} - \bar{\boldsymbol{u}}) d\Gamma = 0. \tag{12}$$

Lagrange multipliers $\boldsymbol{\lambda}$ introduce an additional unknown field defined on the Dirichlet boundary, the interpretation of which in elasticity is the traction, i.e. $\boldsymbol{\lambda} = \boldsymbol{\sigma}(\boldsymbol{u}) \cdot \boldsymbol{n}$ on Γ_D.

The Lagrange multipliers are discretised as follows,

$$\boldsymbol{\lambda}(\boldsymbol{x}) = \sum_{j=1}^{n_d} \boldsymbol{N}_{Lj}(\boldsymbol{x})\boldsymbol{\lambda}_j^e, \tag{13}$$

where the shape functions of the jth node $\boldsymbol{N}_{Lj} = N_{Lj}\boldsymbol{I}_{2\times 2}$ approximates the traction field and $\boldsymbol{\lambda}_j^e = [\lambda_{xj}, \lambda_{yj}]^T$ are the nodal unknown Lagrange multipliers. Following previous notations, the resulting system of matrix equations is

$$\begin{bmatrix} \boldsymbol{K} & \boldsymbol{G} \\ \boldsymbol{G}^T & \boldsymbol{0} \end{bmatrix} \begin{Bmatrix} \boldsymbol{u}^e \\ \boldsymbol{\lambda}^e \end{Bmatrix} = \begin{Bmatrix} \boldsymbol{f} \\ \boldsymbol{f}_L \end{Bmatrix}, \tag{14}$$

where

$$\boldsymbol{G} = \int_{\Gamma_D^e} \boldsymbol{N}^T \boldsymbol{N}_L d\Gamma \qquad \text{and} \qquad \boldsymbol{f}_L = \int_{\Gamma_D^e} \boldsymbol{N}_L^T \bar{\boldsymbol{u}} d\Gamma. \tag{15}$$

As the boundary value function $\bar{\boldsymbol{u}}$ and the displacement field come from the same term in the weak form, it is important that they are approximated using the same shape functions, i.e. $\bar{\boldsymbol{u}} = \boldsymbol{N}\bar{\boldsymbol{u}}^e$, such that

$$\boldsymbol{f}_L = \int_{\Gamma_D^e} \boldsymbol{N}_L^T \boldsymbol{N} d\Gamma \bar{\boldsymbol{u}}^e = \boldsymbol{G}^T \bar{\boldsymbol{u}}^e. \tag{16}$$

We should note that the choice of suitable interpolation spaces for both fields is non-trivial for fictitious domain problems, as the inf-sup condition [26] should be satisfied to achieve stability, which is not the case for most naive choices. Poor performance of the Lagrange multiplier field has been observed as oscillation and locking occurs when interpolation spaces are not properly chosen. Various approaches have been developed to overcome this issue. Barbosa et al. [27] used additional terms to stabilise the original bilinear form. The method of Moës et al. [28] employed a penalty to construct a stable Lagrange multiplier space, leading to a formulation resembling Nitsche's method (see Section 3.1.3). Ramos et al. [6] combined the approach with the extended finite element method and used enrichment functions in the displacement field to ensure stability. The method proposed by Gerstenberger et al. [29] to be introduced in a later section of this article is also a stabilised Lagrange multiplier method, which employs an additional stress field as Lagrange multipliers. A more detailed survey of various approaches to resolve the stability issue for the Lagrange multiplier method can be found in [6].

The Lagrange multiplier method is straightforward and applicable to all kinds of problems, but there are still drawbacks. Besides the non-trivial choice of interpolation space for the multiplier field, the dimension of the final system is increased and the resulting stiffness matrix is no longer positive definite nor banded.

3.1.2. Penalty method

In the classical finite element framework where the mesh aligns with the boundary, the penalty method has been used to prescribe Dirichlet boundary conditions. The method applied to finite elements was first analysed by Babuška [10], including study of the formulation, error estimates and the rate of convergence. The penalty method is also used in meshfree methods [30, 31] and in the finite cell method [32]. Introduced later in this article (Section 3.2.1), the step boundary method appears as another penalty method from the standpoint of numerical analysis.

By introducing a penalty parameter β, the minimisation problem of the modified functional becomes

$$\Pi_{pen}(\boldsymbol{v}) = \Pi(\boldsymbol{v}) + \frac{\beta}{2}\int_{\Gamma_D}(\boldsymbol{v}-\bar{\boldsymbol{u}})^2 d\Gamma \tag{17}$$

and

$$\boldsymbol{u} = \arg\min_{v_i \in \mathscr{H}^1(\Omega)} \Pi_{pen}(\boldsymbol{v}), \tag{18}$$

leading to the weak form statement: find $u_i \in \mathscr{H}^1(\Omega)$ such that

$$\int_\Omega \boldsymbol{\varepsilon}(\delta\boldsymbol{u}) : \boldsymbol{\sigma}(\boldsymbol{u}) d\Omega - \int_\Omega \delta\boldsymbol{u}\cdot\boldsymbol{b} d\Omega - \int_{\Gamma_N}\delta\boldsymbol{u}\cdot\bar{\boldsymbol{g}} d\Gamma + \beta\int_{\Gamma_D}\delta\boldsymbol{u}\cdot(\boldsymbol{u}-\bar{\boldsymbol{u}})d\Gamma = 0. \tag{19}$$

The resulting system of equations is

$$(\boldsymbol{K}+\boldsymbol{K}_p)\boldsymbol{u}^e = \boldsymbol{f}+\boldsymbol{f}_p, \tag{20}$$

where

$$\boldsymbol{K}_p = \beta\int_{\Gamma_D^e}\boldsymbol{N}^T\boldsymbol{N}d\Gamma \qquad \text{and} \qquad \boldsymbol{f}_p = \beta\int_{\Gamma_D^e}\boldsymbol{N}^T\bar{\boldsymbol{u}}d\Gamma. \tag{21}$$

Again the same shape functions as the displacement unknown should be used for the boundary value function, that is

$$\boldsymbol{f}_p = \beta\int_{\Gamma_D^e}\boldsymbol{N}^T\boldsymbol{N}d\Gamma\bar{\boldsymbol{u}}^e = \boldsymbol{K}_p\bar{\boldsymbol{u}}^e. \tag{22}$$

The condition that the penalty method imposes is inconsistent with the original Dirichlet boundary conditions. Integrating the left hand side of (5) by parts gives:

$$\int_\Omega \boldsymbol{\varepsilon}(\delta\boldsymbol{u}) : \boldsymbol{\sigma}(\boldsymbol{u}) d\Omega = \int_{\Gamma_D\cup\Gamma_N}\delta\boldsymbol{u}\cdot\boldsymbol{\sigma}\cdot\boldsymbol{n}d\Gamma - \int_\Omega\delta\boldsymbol{u}\cdot(\nabla\cdot\boldsymbol{\sigma})d\Omega, \tag{23}$$

where for classical finite elements the integral along the Dirichlet boundary vanishes as its test function $\delta\boldsymbol{u}$ vanishes. This no longer holds for displacements selected from $\mathscr{H}^1(\Omega)$ in fictitious domain approaches. In the penalty method, $\int_{\Gamma_D}\delta\boldsymbol{u}\cdot\boldsymbol{\sigma}\cdot\boldsymbol{n}d\Gamma$ together with the simple penalisation $\beta\int_{\Gamma_D}\delta\boldsymbol{u}\cdot(\boldsymbol{u}-\bar{\boldsymbol{u}})d\Gamma$ bring about an approximated condition equivalent to the following strong form condition

$$\boldsymbol{u} + \beta^{-1}\boldsymbol{\sigma}(\boldsymbol{u})\cdot\boldsymbol{n} = \bar{\boldsymbol{u}}, \tag{24}$$

which is variationally inconsistent with the strong form problem statement (1). Lion in the 1960s proved [18] that for each $\beta > 0$ there exists a unique solution $\boldsymbol{u}$ to Problem (19) that converges to the solution of the original problem (5) as $\beta \to +\infty$, which means β should be large enough to obtain a good approximation. Moreover, the variational inconsistency gives rise to suboptimal rates of convergence. Babuška [10] proved the rate of convergence of the order $h^{(2p+1)/3}$ should be achieved in the energy norm when β is taken to be the order of $h^{-(2p+1)/3}$, i.e.

$$\beta = \eta h^{-(2p+1)/3}, \tag{25}$$

where the constant, η, should be large enough to enforce the required boundary condition, h is the grid size and p the polynomial degree of the element bases. For example optimal convergence in

the energy norm for linear elements can be recovered if $\beta = \eta h^{-1}$, but optimality loses with such choice of β in the $\mathscr{L}^2$ norm.

In the penalty method, there are no additional unknowns introduced to the system so the dimension is not increased. The resulting stiffness matrix is symmetric and positive definite provided that β is large enough. However, the drawbacks are that the method is variationally inconsistent as discussed, and β should be chosen from an empirical range, where it is large enough to accurately impose the boundary condition, but not too large that gives rise to ill-conditioning of the stiffness matrix.

3.1.3. Nitsche's method

Since its first introduction in the 1970s [11], Nitsche's method has been employed in meshfree methods [33] and finite element methods with fictitious domains such as spline based approaches [34] and the finite cell method [35]. Nitsche's method posseses features of both Lagrange multiplier and penalty methods. [15] gives a comparison of the three using meshfree methods coupled with finite elements. For fictitious domain finite element methods, a study of stability, error and matrix conditioning is found in [36] and modifications that yield non-symmetric problems but turn out to be robust and efficient were proposed and analysed by Codina et al. [37]. Recent research on the spectral behavior of using Nitsche's method to impose kinematic boundary conditions is found in [38]. Nitsche's method has also been used to deal with embedded interface problems [39], decomposed domains in isogeometric analysis [40, 41] and discontinuous elements in the discontinuous Galerkin method [42], amongst others.

Nitsche's method is stated as

$$\Pi_{Nit}(\boldsymbol{v}) = \Pi(\boldsymbol{v}) - \int_{\Gamma_D} \boldsymbol{\sigma}(\boldsymbol{v}) \cdot \boldsymbol{n} \cdot (\boldsymbol{v} - \bar{\boldsymbol{u}}) d\Gamma + \frac{\beta}{2} \int_{\Gamma_D} (\boldsymbol{v} - \bar{\boldsymbol{u}})^2 d\Gamma \tag{26}$$

and

$$\boldsymbol{u} = \arg \min_{v_i \in \mathscr{H}^1(\Omega)} \Pi_{Nit}(\boldsymbol{v}). \tag{27}$$

Besides a similar penalty term, the new integral along the Dirichlet boundary compared with (17) is added for consistency and symmetry. The corresponding weak form statement is: find $u_i \in \mathscr{H}^1(\Omega)$ such that

$$\begin{aligned} \int_\Omega \boldsymbol{\varepsilon}(\delta \boldsymbol{u}) : \boldsymbol{\sigma}(\boldsymbol{u}) d\Omega - \int_\Omega \delta \boldsymbol{u} \cdot \boldsymbol{b} d\Omega - \int_{\Gamma_N} \delta \boldsymbol{u} \cdot \bar{\boldsymbol{g}} d\Gamma \\ - \int_{\Gamma_D} \delta \boldsymbol{u} \cdot \boldsymbol{\sigma}(\boldsymbol{u}) \cdot \boldsymbol{n} d\Gamma - \int_{\Gamma_D} \boldsymbol{\sigma}(\delta \boldsymbol{u}) \cdot \boldsymbol{n} \cdot (\boldsymbol{u} - \bar{\boldsymbol{u}}) d\Gamma + \beta \int_{\Gamma_D} \delta \boldsymbol{u} \cdot (\boldsymbol{u} - \bar{\boldsymbol{u}}) d\Gamma = 0, \end{aligned} \tag{28}$$

leading to the following system of equations

$$[\boldsymbol{K} + \boldsymbol{K}_p - (\boldsymbol{K}_N + \boldsymbol{K}_N^T)]\boldsymbol{u}^e = \boldsymbol{f} + \boldsymbol{f}_p - \boldsymbol{f}_N, \tag{29}$$

where

$$\boldsymbol{K}_N = \int_{\Gamma_D^e} \boldsymbol{B}^T \boldsymbol{D} \hat{\boldsymbol{n}}^T \boldsymbol{N} d\Gamma \tag{30}$$

and

$$\boldsymbol{f}_N = \int_{\Gamma_D^e} \boldsymbol{B}^T \boldsymbol{D} \hat{\boldsymbol{n}}^T \bar{\boldsymbol{u}} d\Gamma = \boldsymbol{K}_N \bar{\boldsymbol{u}}^e, \tag{31}$$

with $\hat{\boldsymbol{n}}$ being

$$\hat{\boldsymbol{n}} = \begin{bmatrix} n_x & 0 & n_y \\ 0 & n_y & n_x \end{bmatrix}. \tag{32}$$

Performing the same integration by parts as in (23) with the weak form (28), the arised term $\int_{\Gamma_D} \delta\boldsymbol{u} \cdot \boldsymbol{\sigma}(\boldsymbol{u}) \cdot \boldsymbol{n} d\Gamma$ is cancelled out by the first additional term in (28), which gives Nitsche's method variational consistency. The integral along the Dirichlet boundary becomes

$$\int_{\Gamma_D} (\beta\delta\boldsymbol{u} - \boldsymbol{\sigma}(\delta\boldsymbol{u}) \cdot \boldsymbol{n}) \cdot (\boldsymbol{u} - \bar{\boldsymbol{u}}) d\Gamma = 0, \tag{33}$$

which is consistent with the strong form condition, $\boldsymbol{u} = \bar{\boldsymbol{u}}$. The second additional term in Nitsche's weak form ensures symmetry and the last term penalises the displacement.

Nitsche's method is conditionally stable and the value of β should be chosen to assure the coercivity. Nitsche proved that if β is large enough and in proportion to h^{-1}, i.e.

$$\beta = \eta h^{-1} \tag{34}$$

where η is a constant, optimal convergence can be achieved in both $\mathscr{L}^2$ and energy norms. The following stabilisation problem allows an alternative estimation of the critical β. The finite element subspace $\mathscr{V}_h \subset \mathscr{H}^1(\Omega)$ for displacements, which does not fulfil Dirichlet boundary conditions, is considered. Coercivity of Nitsche's bilinear form is assured under the assumption that there exists a mesh-dependent constant $c > 0$ such that

$$||\boldsymbol{\sigma}(\boldsymbol{v}) \cdot \boldsymbol{n}||^2_{\mathscr{L}^2(\Gamma_D)} \leq c||\boldsymbol{v}||^2_{\mathscr{E}(\Omega)}, \tag{35}$$

holds for $\forall v_i \in \mathscr{V}_h$, where the $\mathscr{L}^2$ norm along a boundary and the energy norm over a domain are respectively defined as

$$||\boldsymbol{v}||_{\mathscr{L}^2(\Gamma)} = \left[\int_\Gamma |\boldsymbol{v}|^2 d\Gamma\right]^{1/2} \qquad \text{and} \qquad ||\boldsymbol{v}||_{\mathscr{E}(\Omega)} = \left[\int_\Omega \boldsymbol{\varepsilon}(\boldsymbol{v}) : \boldsymbol{\sigma}(\boldsymbol{v}) d\Omega\right]^{1/2}. \tag{36}$$

The discretisation rewrites the norms in (35) in matrix forms at the element level [43], that is

$$||\boldsymbol{\sigma}(\boldsymbol{v}) \cdot \boldsymbol{n}||^2_{\mathscr{L}^2(\Gamma^e_D)} = \int_{\Gamma^e_D} (\hat{\boldsymbol{n}}\boldsymbol{D}\boldsymbol{B}\boldsymbol{v}^e)^T \hat{\boldsymbol{n}}\boldsymbol{D}\boldsymbol{B}\boldsymbol{v}^e d\Gamma \tag{37}$$

and

$$||\boldsymbol{v}||^2_{\mathscr{E}(\Omega^e)} = \int_{\Omega^e} (\boldsymbol{B}\boldsymbol{v}^e)^T \boldsymbol{D}\boldsymbol{B}\boldsymbol{v}^e d\Omega \geq \int_{\Omega^e_\Gamma} (\boldsymbol{B}\boldsymbol{v}^e)^T \boldsymbol{D}\boldsymbol{B}\boldsymbol{v}^e d\Omega, \tag{38}$$

recalling that $\Omega_\Gamma = \Omega \cap \Omega_{db}$, as described in Section 1.2. [33] suggests the largest eigenvalue calculated from the following problem can be used to estimate the value of c:

$$\mathcal{A}^\Sigma \boldsymbol{x} = \boldsymbol{\Lambda}\mathcal{B}^\Sigma \boldsymbol{x}, \tag{39}$$

where $(\cdot)^\Sigma$ denotes the assembly among elements where

$$\mathcal{A} = \int_{\Gamma^e_D} (\hat{\boldsymbol{n}}\boldsymbol{D}\boldsymbol{B})^T \hat{\boldsymbol{n}}\boldsymbol{D}\boldsymbol{B} d\Gamma \qquad \text{and} \qquad \mathcal{B} = \int_{\Omega^e_\Gamma} \boldsymbol{B}^T \boldsymbol{D}\boldsymbol{B} d\Omega. \tag{40}$$

The largest eigenvalue gives an estimation of $c^2 = \max(\mathbf{\Lambda})$ and Nitsche's method should be stable with the choice $\beta \geq c^2$, providing the same integration scheme is used for $\mathcal{A}$ and $\mathcal{B}$. Note that $\mathcal{A}$ and $\mathcal{B}$ are integrals in elements cut by the Dirichlet boundary, which does not introduce too much additional computational cost.

The major advantages of Nitsche's method are: (a) no additional unknown variable is introduced to the system, (b) variational consistency is satisfied and (c) the penalty parameter can be estimated in advance without too much extra cost. The disadvantage of Nitsche's method comes from the fact that it still includes a penalty parameter in the first place, and the increased parameter according to the grid refinement might eventually be large enough to arouse ill-conditioning in the stiffness matrix. Moreover, when the method is applied in, for instance, the discontinuous Galerkin method, additional calculations are performed which are costly in each element if parameter estimation is needed.

3.1.4. Hellinger-Reissner (H-R) principle

The H-R variational principle is a two-field variational principle in elasticity, theories of which are found in [44, 13]. The hypothesis that test functions vanish on Dirichlet boundaries is not necessary, and Dirichlet boundary conditions can be naturally enforced in finite element methods based on the H-R principle. Hybrid finite element methods can also be derived based on the H-R principle, see e.g. [45, 18]. however, the main advantage of a H-R principle-based method is not in imposing Dirichlet boundary conditions, and its dual fields introduce complexity into both the formulation and the implementation. We introduce the H-R principle here for comparison purposes as it resembles other methods in this article.

The H-R principle is defined on two separate unknown fields (the displacement $\boldsymbol{u}$ and the stress $\boldsymbol{\sigma}$), with both fields being subjected to independent variations. The H-R principle can be stated as

$$\Pi_{H-R}(\boldsymbol{v}, \boldsymbol{\zeta}) = \Pi^*(\boldsymbol{v}, \boldsymbol{\zeta}) - \int_{\Gamma_D} \boldsymbol{\zeta} \cdot \boldsymbol{n} \cdot (\boldsymbol{v} - \bar{\boldsymbol{u}}) d\Gamma \tag{41}$$

and

$$(\boldsymbol{u}, \boldsymbol{\sigma}) = \arg \min_{v_i \in \mathscr{H}^1(\Omega)} \max_{\zeta_{ij} \in \mathscr{L}^2(\Gamma_D)} \Pi_{H-R}(\boldsymbol{v}, \boldsymbol{\zeta}), \tag{42}$$

where $\Pi^*(\boldsymbol{v}, \boldsymbol{\zeta})$ is the counterpart of $\Pi(\boldsymbol{v})$ in Equation (4) but replacing $v_\varepsilon(\boldsymbol{v}) = \frac{1}{2}\boldsymbol{\sigma}(\boldsymbol{v}) : \boldsymbol{\varepsilon}(\boldsymbol{v})$ with $v^*_\varepsilon(\boldsymbol{v}, \boldsymbol{\zeta}) = \boldsymbol{\zeta} : \boldsymbol{\varepsilon}(\boldsymbol{v}) - v_c(\boldsymbol{\zeta})$ (where $v_c(\boldsymbol{\zeta}) = \frac{1}{2}\boldsymbol{\zeta} : \boldsymbol{\varepsilon}(\boldsymbol{\zeta}) = \frac{1}{2}\boldsymbol{\zeta} : (\boldsymbol{C} : \boldsymbol{\zeta})$ is the complementary energy density, with $\boldsymbol{C} = \boldsymbol{E}^{-1}$ being the compliance tensor), that is

$$\Pi^*_p(\boldsymbol{v}, \boldsymbol{\zeta}) = \int_\Omega v^*_\varepsilon(\boldsymbol{v}, \boldsymbol{\zeta}) d\Omega - \int_\Omega \boldsymbol{v} \cdot \boldsymbol{b} d\Omega - \int_{\Gamma_N} \boldsymbol{v} \cdot \bar{\boldsymbol{g}} d\Gamma. \tag{43}$$

The H-R functional (41) leads to the weak form statement: find $u_i \in \mathscr{H}^1(\Omega)$ and $\sigma_{ij} \in \mathscr{L}^2(\Omega)$ such that

$$\int_\Omega \boldsymbol{\varepsilon}(\delta\boldsymbol{u}) : \boldsymbol{\sigma} d\Omega - \int_\Omega \delta\boldsymbol{\sigma} : (\boldsymbol{\varepsilon}(\boldsymbol{\sigma}) - \boldsymbol{\varepsilon}(\boldsymbol{u})) d\Omega - \int_\Omega \delta\boldsymbol{u} \cdot \boldsymbol{b} d\Omega - \int_{\Gamma_N} \delta\boldsymbol{u} \cdot \bar{\boldsymbol{g}} d\Gamma$$
$$- \int_{\Gamma_D} \delta\boldsymbol{u} \cdot \boldsymbol{\sigma} \cdot \boldsymbol{n} d\Gamma - \int_{\Gamma_D} \delta\boldsymbol{\sigma} \cdot \boldsymbol{n} \cdot (\boldsymbol{u} - \bar{\boldsymbol{u}}) d\Gamma = 0. \tag{44}$$

The discretisation of the stress field is given as follows,

$$\boldsymbol{\sigma}(\boldsymbol{x}) = \sum_{j=1}^{n_d} \boldsymbol{N}_{sj}(\boldsymbol{x})\boldsymbol{\sigma}_j^e, \tag{45}$$

where $\boldsymbol{N}_{sj} = N_{sj}\boldsymbol{I}_{3\times 3}$ is the shape functions of the jth node for the stress. $\boldsymbol{\sigma}_j^e = [\sigma_{xj}, \sigma_{yj}, \tau_{xyj}]^T$ are nodal unknowns of the stress. The resulting system of equations is

$$\begin{bmatrix} \boldsymbol{0} & \boldsymbol{A}_s \\ \boldsymbol{A}_s^T & -\boldsymbol{K}_s \end{bmatrix} \begin{Bmatrix} \boldsymbol{u}^e \\ \boldsymbol{\sigma}^e \end{Bmatrix} = \begin{Bmatrix} \boldsymbol{f} \\ -\boldsymbol{f}_s \end{Bmatrix}, \tag{46}$$

where

$$\boldsymbol{K}_s = \int_{\Omega^e} \boldsymbol{N}_s^T \boldsymbol{S} \boldsymbol{N}_s d\Omega \qquad \text{and} \qquad \boldsymbol{A}_s = \int_{\Omega^e} \boldsymbol{B}^T \boldsymbol{N}_s d\Omega - \boldsymbol{G}_s, \tag{47}$$

with $\boldsymbol{S}$ denoting the compliance matrix,

$$\boldsymbol{G}_s = \int_{\Gamma_D^e} \boldsymbol{N}^T \hat{\boldsymbol{n}} \boldsymbol{N}_s d\Gamma \tag{48}$$

and

$$\boldsymbol{f}_s = \int_{\Gamma_D^e} \boldsymbol{N}_s^T \hat{\boldsymbol{n}}^T \bar{\boldsymbol{u}} d\Gamma = \boldsymbol{G}_s^T \bar{\boldsymbol{u}}^e. \tag{49}$$

As the stress field is discontinuous across the element boundary, it can be condensed at the element level, such that from (46), we have

$$\boldsymbol{\sigma}^e = \boldsymbol{A}_s^{-1} \boldsymbol{f}, \tag{50}$$

and (46) is left with just displacement unknowns, that is

$$\boldsymbol{A}_s^T \boldsymbol{u}^e = \boldsymbol{K}_s \boldsymbol{A}_s^{-1} \boldsymbol{f} - \boldsymbol{f}_s. \tag{51}$$

In other words, there are no additional variables in the resulting formation after assembly.

Hybrid finite elements using the H-R principle have advantages for specific problems in plate analysis, and do not have the problem of shear and volumetric locking as in standard displacement elements. Dirichlet boundary conditions are enforced naturally in the method, but its intrinsic complexity in formulation has restricted its application.

3.1.5. Linked Lagrange multiplier (LLM) method

The so called LLM method, proposed by Gerstenberger et al. [29], is a new strategy of imposing Dirichlet boundary conditions which uses an additional stress field that act as Lagrange multipliers. The LLM method has been further modified to achieve symmetry and consistency [12].

The original LLM method [29] modifies the weak form directly, leading to a non-symmetric form. The weak form statement is: find $u_i \in \mathscr{H}^1(\Omega)$ and $\sigma_{ij} \in \mathscr{L}^2(\Omega)$ such that

$$\int_\Omega \boldsymbol{\varepsilon}(\delta\boldsymbol{u}) : \boldsymbol{\sigma}(\boldsymbol{u}) d\Omega - \int_\Omega \delta\boldsymbol{\sigma} \cdot (\boldsymbol{\varepsilon}(\boldsymbol{\sigma}) - \boldsymbol{\varepsilon}(\boldsymbol{u})) d\Omega - \int_\Omega \delta\boldsymbol{u} \cdot \boldsymbol{b} d\Omega - \int_{\Gamma_N} \delta\boldsymbol{u} \cdot \bar{\boldsymbol{g}} d\Gamma$$
$$- \int_{\Gamma_D} \delta\boldsymbol{u} \cdot \boldsymbol{\sigma} \cdot \boldsymbol{n} d\Gamma - \int_{\Gamma_D} \delta\boldsymbol{\sigma} \cdot \boldsymbol{n} \cdot (\boldsymbol{u} - \bar{\boldsymbol{u}}) d\Gamma = 0. \tag{52}$$

The approach seems to be inspired by the two-field H-R principle and the Lagrange multiplier method. Classical Lagrange multipliers are defined on the boundary and is coupled with the other displacement field only on the Dirichlet boundary. The LLM approach shifts Lagrange multipliers into the domain, and it is easily seen from the second integral in Equation (52) that the two unknown fields are weakly linked. But in this approach the first term of the strain energy in Equation (52) is still derived from the displacement field, which is the main difference from the H-R principle.

Given that the stress, and its test function, are discretised in the same way as (45), the resulting system is

$$\begin{bmatrix} \boldsymbol{K} & -\boldsymbol{G}_s \\ \boldsymbol{A}_s^T & -\boldsymbol{K}_s \end{bmatrix} \begin{Bmatrix} \boldsymbol{u}^e \\ \boldsymbol{\sigma}^e \end{Bmatrix} = \begin{Bmatrix} \boldsymbol{f} \\ -\boldsymbol{f}_s \end{Bmatrix}, \tag{53}$$

where the matrices in the system have the same expanded expressions as Equation (47)-(49). As the stress field is discontinuous across inter-element boundaries, the system can be similarly condensed at the element level as with the H-R principle, giving rise to

$$(\boldsymbol{K} + \boldsymbol{G}_s \boldsymbol{K}_s^{-1} \boldsymbol{A}_s^T)\boldsymbol{u}^e = \boldsymbol{f} + \boldsymbol{G}_s \boldsymbol{K}_s^{-1} \boldsymbol{f}_s \tag{54}$$

Since the main inconvenience of the method is its non-symmetric matrix, a fully symmetric formulation was later derived and is detailed below.

In [12] the Poisson equation is considered, and the unknown stress field is defined in Ω_Γ (defined as $\Omega \cap \Omega_{db}$ as shown in Figure 1) on the discretised grid near the Dirichlet boundary. A continuous version of the saddle point problem of the energy functional can be written as

$$\Pi_{LLM}(\boldsymbol{v}, \boldsymbol{\zeta}) = \Pi(\boldsymbol{v}) - \int_{\Gamma_D} \boldsymbol{\zeta} \cdot \boldsymbol{n} \cdot (\boldsymbol{v} - \bar{\boldsymbol{u}}) d\Gamma - \frac{1}{2m} \int_{\Omega_\Gamma} \boldsymbol{E} : (\boldsymbol{\varepsilon}(\boldsymbol{\zeta}) - \boldsymbol{\varepsilon}(\boldsymbol{v}))^2 d\Omega \tag{55}$$

and

$$(\boldsymbol{u}, \boldsymbol{\sigma}) = \arg \min_{v_i \in \mathscr{H}^1(\Omega)} \max_{\zeta_{ij} \in \mathscr{L}^2(\Omega)} \Pi_{LLM}(\boldsymbol{v}, \boldsymbol{\zeta}). \tag{56}$$

The first additional term in (55) introduces the stress field as Lagrange multipliers, and the second additional term couples the two fields near the Dirichlet boundary (in Ω_Γ) in a least square sense, where m is a penalty-type parameter. However importantly, it has been proved that the method is stable for $m > 1$. The corresponding weak form statement is: find $u_i \in \mathscr{H}^1(\Omega)$ and $\sigma_{ij} \in \mathscr{L}^2(\Omega)$ such that

$$\begin{aligned} \int_\Omega \boldsymbol{\varepsilon}(\delta \boldsymbol{u}) : \boldsymbol{\sigma}(\boldsymbol{u}) d\Omega - \frac{1}{m} \left[\int_{\Omega_\Gamma} \delta \boldsymbol{\sigma} : (\boldsymbol{\varepsilon}(\boldsymbol{\sigma}) - \boldsymbol{\varepsilon}(\boldsymbol{u})) d\Omega - \int_{\Omega_\Gamma} \boldsymbol{\varepsilon}(\delta \boldsymbol{u}) : (\boldsymbol{\sigma} - \boldsymbol{\sigma}(\boldsymbol{u})) d\Omega \right] \\ - \int_\Omega \delta \boldsymbol{u} \cdot \boldsymbol{b} d\Omega - \int_{\Gamma_N} \delta \boldsymbol{u} \cdot \bar{\boldsymbol{g}} d\Gamma - \int_{\Gamma_D} \delta \boldsymbol{u} \cdot \boldsymbol{\sigma} \cdot \boldsymbol{n} d\Gamma - \int_{\Gamma_D} \delta \boldsymbol{\sigma} \cdot \boldsymbol{n} \cdot (\boldsymbol{u} - \bar{\boldsymbol{u}}) d\Gamma = 0. \end{aligned} \tag{57}$$

Given that the stress field and the test function are discretised the same as (45), the resulting system of matrix equations is

$$\begin{bmatrix} \boldsymbol{K} - \boldsymbol{K}_\Gamma & \boldsymbol{A}_{s2} \\ \boldsymbol{A}_{s2}^T & -\boldsymbol{K}_{s2} \end{bmatrix} \begin{Bmatrix} \boldsymbol{u}^e \\ \boldsymbol{\sigma}^e \end{Bmatrix} = \begin{Bmatrix} \boldsymbol{f} \\ -\boldsymbol{f}_s \end{Bmatrix}, \tag{58}$$

where

$$\boldsymbol{K}_\Gamma = \frac{1}{m} \int_{\Omega_\Gamma^e} \boldsymbol{B}^T \boldsymbol{D} \boldsymbol{B} d\Omega, \qquad \boldsymbol{K}_{s2} = \frac{1}{m} \int_{\Omega_\Gamma^e} \boldsymbol{N}_s^T \boldsymbol{S} \boldsymbol{N}_s d\Omega \tag{59}$$

and

$$\boldsymbol{A}_{s2} = \frac{1}{m} \int_{\Omega_\Gamma^e} \boldsymbol{B}^T \boldsymbol{N}_s d\Omega - \boldsymbol{G}_s. \tag{60}$$

Similarly, the discontinuous stress across element boundaries allows condensation, giving rise to

$$(\boldsymbol{K} - \boldsymbol{K}_\Gamma + \boldsymbol{A}_{s2} \boldsymbol{K}_{s2}^{-1} \boldsymbol{A}_{s2}^T) \boldsymbol{u}^e = \boldsymbol{f} - \boldsymbol{A}_{s2} \boldsymbol{K}_{s2}^{-1} \boldsymbol{f}_s \tag{61}$$

and this system of equations is symmetric and banded.

The stability of the LLM method in a variety of elliptic problems have been analysed in [46], the optimal convergence order being recovered for most cases. Providing $m > 1$, the LLM method has been proved to be stable for simple choices of interpolation space pairs: (a) equal order interpolation and (b) the displacement and the stress fields being piecewise linear and piecewise constant respectively. There are no additional variables introduced to the system, although the condensation process of the stress field for elements cut by the Dirichlet boundary, which includes the inversion of the compliance matrix $\boldsymbol{K}_{s2}$, introduces extra computational cost.

3.2. Implicit boundary method

The idea of using implicit boundary functions to satisfy boundary conditions in the finite element method can be traced back to the work of Kantorovich and Krylov [21]. This approach was referred to as the "implicit boundary method" by Kumar et al. in [5]. Here, we follow the use of this term and the approach proposed in the same article that uses approximate step functions as implicit boundary functions is referred to as the "step boundary method" [47] in this article, discussed in Section 3.2.1.

The implicit boundary method modifies the interpolation of the unknown field to transform the geometric boundary information into analytical equations, and the original variational principle can be employed without modification. The essential idea is to employ a weighted form for, e.g. a scalar unknown field u:

$$u = \omega \psi \tag{62}$$

where ψ is the usual approximation of the unknown field and ω is the implicit weight function (also known as the Dirichlet function) that has $\mathscr{C}^1$ continuity and satisfies:

$$\begin{cases} \omega > 0, & \text{in } \Omega \backslash \Gamma_D \\ \omega = 0, & \text{on } \Gamma_D \end{cases} \tag{63}$$

The early work of Kharrik [48] proved the completeness of (62). Rvachev et al. [49] developed the R-function method to construct exact implicit functions for general boundary conditions. Shapiro et al. [50] provided theories on automatically constructed, differentiated and integrated R-functions. The WEB method [51, 20] adopted the weighted form in the B-spline-based finite element method, allowing the Dirichlet problem to be solved on a regular background mesh.

The weak form (5) is employed here without further restrictions. For a two-dimensional finite element problem, weighted displacements can be written as

$$\boldsymbol{u} = \boldsymbol{W} \boldsymbol{u}_g + \boldsymbol{u}_a \qquad \text{and} \qquad \delta \boldsymbol{u} = \boldsymbol{W} \delta \boldsymbol{u}_g, \tag{64}$$

in which the weight matrix $\boldsymbol{W} = \text{diag}(\omega_x, \omega_y)$, $\boldsymbol{u}_g = [u_{gx}, u_{gy}]^T$ is the grid unknown, and $\boldsymbol{u}_a = [u_{ax}, u_{ay}]^T$ is the boundary value function that satisfies the inhomogeneous Dirichlet boundary conditions.

The same discretisation as the classical finite element for the grid unknown $\boldsymbol{u}_g$ and test function $\delta\boldsymbol{u}_g$ leads to the following forms of real and virtual displacements

$$\boldsymbol{u} = \boldsymbol{W}\boldsymbol{N}\boldsymbol{u}_g^e + \boldsymbol{u}_a \qquad \text{and} \qquad \delta\boldsymbol{u} = \boldsymbol{W}\boldsymbol{N}\delta\boldsymbol{u}_g^e. \tag{65}$$

Strains and the stress become

$$\boldsymbol{\varepsilon}(\boldsymbol{u}) = \mathcal{L}(\boldsymbol{u}) = \hat{\boldsymbol{B}}\boldsymbol{u}_g^e + \mathcal{L}(\boldsymbol{u}_a), \qquad \boldsymbol{\varepsilon}(\delta\boldsymbol{u}) = \mathcal{L}(\delta\boldsymbol{u}) = \hat{\boldsymbol{B}}\delta\boldsymbol{u}_g^e \tag{66}$$

and

$$\boldsymbol{\sigma}(\boldsymbol{u}) = \boldsymbol{D}\boldsymbol{\varepsilon}(\boldsymbol{u}) = \boldsymbol{D}\hat{\boldsymbol{B}}\boldsymbol{u}_g^e + \boldsymbol{D}\mathcal{L}(\boldsymbol{u}_a). \tag{67}$$

The modified strain-displacement matrix is given by

$$\hat{\boldsymbol{B}} = \mathcal{L}(\boldsymbol{W}\boldsymbol{N}), \tag{68}$$

leading to the following system

$$\hat{\boldsymbol{K}}\boldsymbol{u}_g^e = \hat{\boldsymbol{f}} - \boldsymbol{f}_{ib}, \tag{69}$$

where

$$\hat{\boldsymbol{K}} = \int_{\Omega^e} \hat{\boldsymbol{B}}^T\boldsymbol{D}\hat{\boldsymbol{B}}d\Omega, \qquad \hat{\boldsymbol{f}} = \int_{\Omega^e} \boldsymbol{N}^T\boldsymbol{W}\boldsymbol{b}d\Omega + \int_{\Gamma_N^e} \boldsymbol{N}^T\boldsymbol{W}\bar{\boldsymbol{g}}d\Gamma. \tag{70}$$

and

$$\boldsymbol{f}_{ib} = \int_{\Omega^e} \hat{\boldsymbol{B}}^T\boldsymbol{D}\mathcal{L}(\boldsymbol{u}_a)d\Omega. \tag{71}$$

Unlike the boundary value function $\bar{\boldsymbol{u}}$ in previous sections, $\boldsymbol{u}_a$ here is defined over the physical domain. As the system solves for the discretised grid unknowns $\boldsymbol{u}_g$, the correct displacement should be recovered through (64) after solution. Owing to this feature, a smoothly constructed $\boldsymbol{u}_a$ that satisfies the inhomogeneous Dirichlet boundary conditions without being approximated on the grid leads to a more accurate solution. For example, the transfinite interpolation technique [16] has been used to construct the required boundary value function in the finite cell method.

The implicit boundary method is a straightforward method that is easy to understand. It represents Dirichlet boundary conditions without losing accuracy, and does not have artificial parameters in the formulation. However, a smooth weighting function for the whole physical domain is need and its gradient calculated, which requires costly construction techniques for complex geometries. And, there is no direct way to impose partially prescribed boundary conditions in the implicit boundary method.

3.2.1. Step boundary method

Kumar et al. [52] proposed the step boundary method in fictitious domain finite element analysis. The step boundary method has a similar formulation to the implicit boundary method but ends up with a system that contains a penalty parameter. It has also been applied to spline based finite element methods [53] and the material point method [54].

The following function, which vanishes on the Dirichlet boundary and rises to unity within the step size ϵ, is an example of the numerically constructed step-like functions employed in the step boundary method

$$\omega(\phi) = 1 - \max(0, 1 - \phi/\epsilon)^\kappa, \tag{72}$$

where $\phi = dist(\boldsymbol{x}, \Gamma_D)$ denotes the distance from the boundary. The step size ϵ controls the size of the transition and κ controls the smoothness. The function tends to the Heaviside step function in the limit as $\epsilon \to 0$. Such functions have been employed in the WEB method, but in the step boundary method, ϵ is restricted to be very small compared to the element length, h, which generates a large gradient near the Dirichlet boundary. The large gradient acts as a penalty factor that penalises grid unknowns in the final system of equations, which links the step boundary method to the original penalty method.

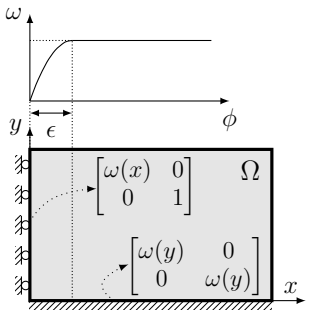

Figure 3: The Dirichlet function and a domain with roller and fully fixed boundaries.

As a result of the small step size, the displacement inside the area where $\phi > \epsilon$ remain unchanged, and Dirichlet functions can be defined locally in each element cut by the Dirichlet boundary. This feature allows the imposition of partially prescribed conditions in the step boundary method. We denote $\boldsymbol{W} = \text{diag}(\omega_x, \omega_y)$ here and ω_x or ω_y equals to either unity or the Dirichlet function $\omega(\phi)$ depending on the condition in each direction. Figure 3 shows an example domain with a roller boundary at $x = 0$ and a fully fixed boundary at $y = 0$ with respective weight matrices; ω_y at $x = 0$ is set to unity as the tangential displacement is unconstrained.

The formulation of element stiffness matrix $\hat{\boldsymbol{K}}$ can be simplified owing to the nature of the step-like Dirichlet function. For conciseness, the $\hat{\boldsymbol{B}}$ matrix is decomposed at the node level,

$$\hat{\boldsymbol{B}} = \left[\hat{\boldsymbol{B}}_1 \ \hat{\boldsymbol{B}}_2 \ \cdots \ \hat{\boldsymbol{B}}_{n_d}\right], \tag{73}$$

where n_d is the number of nodes in a single element. The decomposed $\hat{\boldsymbol{B}}_j$ $(j = 1, 2, ..., n_d)$ can be further expanded as

$$\hat{\boldsymbol{B}}_j = \mathcal{L}(\boldsymbol{W}\boldsymbol{N}_j) = \mathcal{L}(\boldsymbol{N}_j)\boldsymbol{W} + \mathcal{L}(\boldsymbol{W})\boldsymbol{N}_j = \boldsymbol{B}_{1j} + \boldsymbol{B}_{2j}, \tag{74}$$

which includes two parts that respectively contain gradients of Dirichlet boundary functions and shape functions, where

$$\boldsymbol{B}_{1j} = \begin{bmatrix} \omega_x \frac{\partial N_j}{\partial x} & 0 \\ 0 & \omega_y \frac{\partial N_j}{\partial y} \\ \omega_x \frac{\partial N_j}{\partial y} & \omega_y \frac{\partial N_j}{\partial x} \end{bmatrix} \qquad \text{and} \qquad \boldsymbol{B}_{2j} = \begin{bmatrix} N_j \frac{\partial \omega_n}{\partial x} & 0 \\ 0 & N_j \frac{\partial \omega_y}{\partial y} \\ N_j \frac{\partial \omega_x}{\partial y} & N_j \frac{\partial \omega_y}{\partial x} \end{bmatrix}. \tag{75}$$

The element stiffness matrix is then decomposed as

$$\hat{\boldsymbol{K}} = \boldsymbol{K}_1 + \boldsymbol{K}_2^T + \boldsymbol{K}_2 + \boldsymbol{K}_3, \tag{76}$$

where

$$\boldsymbol{K}_1 = \int_{\Omega^e} \boldsymbol{B}_1^T \boldsymbol{D} \boldsymbol{B}_1 d\Omega, \quad \boldsymbol{K}_2 = \int_{\Omega^e} \boldsymbol{B}_1^T \boldsymbol{D} \boldsymbol{B}_2 d\Omega \quad \text{and} \quad \boldsymbol{K}_3 = \int_{\Omega^e} \boldsymbol{B}_2^T \boldsymbol{D} \boldsymbol{B}_2 d\Omega. \tag{77}$$

The Dirichlet function (72) generates the large gradient $\partial\omega/\partial\phi$ within the narrow banded area near the Dirichlet boundary ($\phi < \epsilon$) as a result of the tiny step size ϵ. It rises to a plateau of unity at the distance ϵ such that $\partial\omega/\partial\phi = 0$ on the plateau. Such properties allow following simplifications:

- integrals over the problem domain containing $\partial\omega/\partial\phi$, e.g. $\boldsymbol{K}_2$ and $\boldsymbol{K}_3$, can be integrated in the narrow band in local tangential coordinates;
- the contribution of the Dirichlet function itself is negligible if integrals over the problem domain do not involve $\partial\omega/\partial\phi$, e.g. $\boldsymbol{K}_1$; and
- values of the shape function N_j barely vary across the narrow band.

As a result, we have $\boldsymbol{K}_1 = \boldsymbol{K}$ and $\hat{\boldsymbol{f}} = \boldsymbol{f}$. It has been shown in general that the effect of $\boldsymbol{K}_2$ is negligible [55], as it is relatively small compared to $\boldsymbol{K}_3$ which includes the product of two $\mathcal{L}(\boldsymbol{W})$. The rest of the stiffness matrix can be expressed as

$$\boldsymbol{K}_{stp} = \boldsymbol{K}_3 = \int_{\Gamma_D^e} \boldsymbol{N}^T \int_0^{\epsilon} \mathcal{L}(\boldsymbol{W})^T \boldsymbol{D} \mathcal{L}(\boldsymbol{W}) dn \boldsymbol{N} dt. \tag{78}$$

The final system of equations is

$$(\boldsymbol{K} + \boldsymbol{K}_{stp}) \boldsymbol{u}_g^e = \boldsymbol{f} - \boldsymbol{f}_{ib}. \tag{79}$$

In the step boundary method, using the same approximation $\boldsymbol{u}_a = \boldsymbol{N}\boldsymbol{u}_a^e$ as the grid variable further simplifies calculation and avoids poor convergence rates. With the introduced simplifications, we have $\boldsymbol{f}_{ib} = \boldsymbol{f}_{stp}$, that is

$$\boldsymbol{f}_{stp} = \int_{\Omega^e} (\boldsymbol{B}_1 + \boldsymbol{B}_2)^T \boldsymbol{D} \boldsymbol{B} \boldsymbol{u}_a^e d\Omega = \boldsymbol{K} \boldsymbol{u}_a^e. \tag{80}$$

The step boundary method inherits the straightforward formulation of the implicit boundary method, and can be considered as a method that renders the original penalty method with an evident physical interpretation. The method is also capable of imposing partially prescribed boundaries. However, the drawbacks are that it possesses a similar inconsistency as in the penalty method, as observed numerically (cf. Section 5), and the step size ϵ must be chosen empirically to achieve good performance.

3.3. Fat Boundary Method

As mentioned above, the fat boundary method is a multidomain approach developed for domains with constrained holes, and as such the problem setting is slightly different (see Figure 4(a)), where Ω denotes the domain of interest. The fictitious domain Ω_{fict}, as shown in Figure 4(b), is Lipschitz bounded and $\Omega_o \subset \Omega_{fict}$ is a collection of smooth subsets. The boundaries are denoted

by $\partial\Omega_{fict} = \Gamma$ and $\partial\Omega_o = \Gamma_D$, and we denote that $\bar{\Omega}_o = \Omega_o \backslash \Gamma_D$, such that $\Omega = \Omega_{fict} \backslash \bar{\Omega}_o$. The following functional spaces are employed here

$$\mathscr{H}^1_{\Gamma}(\Omega) = \{v_i \in \mathscr{H}^1(\Omega) | \boldsymbol{v} = \boldsymbol{0} \text{ on } \Gamma\} \qquad \text{and} \qquad \mathscr{H}^1_{\Gamma_D}(\Omega) = \{v_i \in \mathscr{H}^1(\Omega) | \boldsymbol{v} = \bar{\boldsymbol{u}} \text{ on } \Gamma_D\}. \quad (81)$$

The model problem of elasticity is stated as: find $u_i \in \mathscr{H}^1_0(\Omega \backslash \bar{B})$ such that

$$-\nabla \cdot \boldsymbol{\sigma}(\boldsymbol{u}) = \boldsymbol{b} \quad \text{in } \Omega \qquad \text{and} \qquad \boldsymbol{u} = \bar{\boldsymbol{u}} \quad \text{on } \Gamma_D. \quad (82)$$

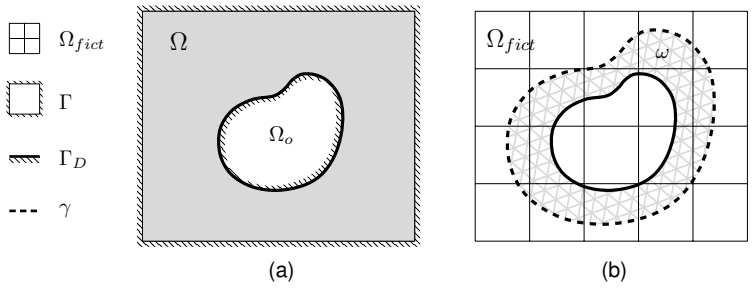

Figure 4: Domain setting and discretisation of the fat boundary method.

By introducing an artificial boundary zone ω containing Γ_D (Figure 4(b)), the initial problem is split into two coupled sub-problems. The crust-like area ω is delimited by Γ_D and γ, and then meshed locally, while the fictitious domain Ω_{fict} is capable of having, e.g. a Cartesian mesh. Let $\bar{\boldsymbol{u}}^{\chi}$ be a harmonic extension of $\bar{\boldsymbol{u}}$ in Ω_o and $\boldsymbol{b}^{\chi}$ be $\boldsymbol{b}$ with the extension $\boldsymbol{0}$ in Ω_o, and (82) can be replaced equivalently by: find $(d_i, \hat{u}_i) \in \mathscr{H}^1_{\Gamma_D}(\omega) \times \mathscr{H}^1_{\Gamma}(\Omega_{fict})$ such that

$$\begin{cases} (a): & -\nabla \cdot \boldsymbol{\sigma}(\boldsymbol{d}) = \boldsymbol{b} \quad \text{in } \omega \qquad \text{and} \qquad \boldsymbol{d} = \hat{\boldsymbol{u}} \quad \text{on } \gamma, \\ (b): & -\nabla \cdot \boldsymbol{\sigma}(\hat{\boldsymbol{u}}) = \boldsymbol{b}^{\chi} + \delta_{\Gamma_D}(\boldsymbol{\sigma}(\boldsymbol{d}) - \boldsymbol{\sigma}^{\chi}(\bar{\boldsymbol{u}}^{\chi})) \cdot \boldsymbol{n} \quad \text{in } \Omega_{fict}, \end{cases} \quad (83)$$

where $\hat{\boldsymbol{u}}$ and $\boldsymbol{d}$ denote respective displacement fields defined in Ω_{fict} and ω for the sub-problems. Note that $\boldsymbol{\sigma}(\cdot)$ here represent stress tensors calculated from different displacement fields (and strain tensors $\boldsymbol{\varepsilon}(\cdot)$ similarly). $\boldsymbol{\sigma}^{\chi}$ is the stress calculated from $\bar{\boldsymbol{u}}^{\chi}$, which becomes a known function to the system and vanishes in the case of a homogeneous boundary condition, and cases in which no analytical harmonic extension to $\bar{\boldsymbol{u}}$ can be found are also discussed in [14]. δ_{Γ_D} is a Kronecker delta function which takes unity on Γ_D and vanishes elsewhere. The proof of the equivalence of problems (82) and (83) is provided in [14].

The two sub-problems are linked by (a) setting $\boldsymbol{d} = \hat{\boldsymbol{u}}$ on the artificial boundary γ and (b) the additional term $\delta_{\Gamma_D}(\boldsymbol{\sigma}(\boldsymbol{d}) - \boldsymbol{\sigma}^{\chi}) \cdot \boldsymbol{n}$ in Ω, which prescribes the jump of the normal stress across Γ_D, such that Dirichlet boundary conditions are weakly enforced in the computation of the fictitious domain. The weak form of (83) can be stated as: find $(d_i, \hat{u}_i) \in \mathscr{H}^1_{\Gamma_D}(\omega) \times \mathscr{H}^1_{\Gamma}(\Omega_{fict})$ such that

$$\begin{cases} (a): & \displaystyle\int_{\omega} \boldsymbol{\varepsilon}(\delta\boldsymbol{d}) : \boldsymbol{\sigma}(\boldsymbol{d}) d\Omega = \int_{\omega} \delta\boldsymbol{d} \cdot \boldsymbol{b} d\Omega \qquad \text{and} \qquad \boldsymbol{d}|_{\gamma} = \hat{\boldsymbol{u}}|_{\gamma}, \\ (b): & \displaystyle\int_{\Omega_{fict}} \boldsymbol{\varepsilon}(\delta\hat{\boldsymbol{u}}) : \boldsymbol{\sigma}(\hat{\boldsymbol{u}}) d\Omega = \int_{\Omega_{fict}} \delta\hat{\boldsymbol{u}} \cdot \boldsymbol{b}^{\chi} d\Omega + \int_{\Gamma_D} \delta\hat{\boldsymbol{u}} \cdot (\boldsymbol{\sigma}(\boldsymbol{d}) - \boldsymbol{\sigma}^{\chi}(\bar{\boldsymbol{u}}^{\chi})) \cdot \boldsymbol{n} d\Gamma. \end{cases} \quad (84)$$

The original weak form (5) is employed without modification for each sub-problem. It is also worth noting that analytical solutions to (84)(a) can be used if they exist in certain cases, which leads to

a semi-discrete fat boundary method [56]. The fully discretised fat boundary method is analysed in [57], with both sub-problems being discretised with finite elements. In the fully discrete approach a fixed point algorithm can be used to solve the sub-problems alternately and iteratively. The iterative procedure of Problem (84) for a given solution step $k > 0$ is:

- solving (a) for $\boldsymbol{d}^k$ under the condition of $\boldsymbol{d}^k|_\gamma = \hat{\boldsymbol{u}}^{k-1}|_\gamma$ from the last step; and
- solving (b) for $\hat{\boldsymbol{u}}^k$ with the jump of stress in the last integral in (84) being $\boldsymbol{\sigma}(\boldsymbol{d}^k) - \boldsymbol{\sigma}^\chi$.

A relaxation parameter r^* may be added to (84)(a) to improve accuracy and convergence, leading to the modified boundary condition for step k: $\boldsymbol{d}^k|_\gamma = r^*\boldsymbol{d}^{k-1}|_\gamma + (1 - r^*)\hat{\boldsymbol{u}}^k|_\gamma$. A detailed study of relaxation and iterative solution techniques in the fat boundary method is provided in [14].

Employing the same discretisation as previous sections for both sub-problems, the systems of equations for the fully discrete approach can be expressed in the following form:

$$\begin{cases} (a): & \boldsymbol{K}_{(a)}\boldsymbol{d}^e = \boldsymbol{f}_{(a)}, \\ (b): & \boldsymbol{K}_{(b)}\hat{\boldsymbol{u}}^e = \boldsymbol{f}_{(b)} + \boldsymbol{f}_{at}, \end{cases} \tag{85}$$

where $\boldsymbol{K}_{(\cdot)}$ and $\boldsymbol{f}_{(\cdot)}$ remain the same formulation as in the classical finite element method (9), and

$$\boldsymbol{f}_{at} = \int_{\Gamma_D^e} \boldsymbol{N}^T \hat{\boldsymbol{n}}(\boldsymbol{\sigma}(\boldsymbol{d}) - \boldsymbol{\sigma}^\chi) d\Gamma, \tag{86}$$

with the known quantity $(\boldsymbol{\sigma}(\boldsymbol{d}) - \boldsymbol{\sigma}^\chi)$ being calculated from the solution of (85)(a) and the constructed boundary value extension.

The fat boundary method is capable of dealing with a large number of holes in a single model, especially when the holes have identical geometry, the same discretisation can be used for every hole and the stiffness matrix needs to be stored only once. In each iteration, the local finite element problems are solved separately, which naturally fits into a parallel solution environment. Analytical solutions of local problems can also be used if they exist, which increases accuracy and efficiency. Although the method requires an iterative solution procedure, it is efficient and is capable of providing an accurate solution in the neighbourhood of the holes while using a relatively coarse mesh for the fictitious domain.

3.4. Summary

For convenience, and since it appears not to have been presented this way before, the energy functionals and the respective solution systems of the introduced methods are summarised in Tables 1-2 respectively. The subscript texts "ib", "stp" and "fat" stand for the implicit boundary method, the step boundary method and the fat boundary method respectively.

4. Inclined and partially prescribed boundary conditions

The partially prescribed boundary conditions described in (1), especially roller boundary conditions, are useful in practical engineering applications. However, the introduced formulations in previous sections do not take into account the case when a local coordinate axis x_i' of the partially prescribed boundary is not parallel to one of the global coordinate axes, and previous research on imposing such boundary conditions with these weak imposition methods is hard to find. In this

Table 1: Energy functionals

denotation	energy functional
$\Pi_L(\boldsymbol{v},\boldsymbol{\gamma})$	$\Pi(\boldsymbol{v}) + \int_{\Gamma_D} \boldsymbol{\gamma}\cdot(\boldsymbol{v}-\bar{\boldsymbol{u}})d\Gamma$
$\Pi_{pen}(\boldsymbol{v})$	$\Pi(\boldsymbol{v}) + \frac{\beta}{2}\int_{\Gamma_D} (\boldsymbol{v}-\bar{\boldsymbol{u}})^2 d\Gamma$
$\Pi_{Nit}(\boldsymbol{v})$	$\Pi(\boldsymbol{v}) - \int_{\Gamma_D} \boldsymbol{\sigma}(\boldsymbol{v})\cdot\boldsymbol{n}\cdot(\boldsymbol{v}-\bar{\boldsymbol{u}})d\Gamma + \frac{\beta}{2}\int_{\Gamma_D}(\boldsymbol{v}-\bar{\boldsymbol{u}})^2 d\Gamma$
$\Pi_{H-R}(\boldsymbol{v},\boldsymbol{\zeta})$	$\Pi^*(\boldsymbol{v},\boldsymbol{\zeta}) - \int_{\Gamma_D}\boldsymbol{\zeta}\cdot\boldsymbol{n}\cdot(\boldsymbol{v}-\bar{\boldsymbol{u}})d\Gamma$
$\Pi_{LLM}(\boldsymbol{v},\boldsymbol{\zeta})$	$\Pi(\boldsymbol{v}) - \int_{\Gamma_D}\boldsymbol{\zeta}\cdot\boldsymbol{n}\cdot(\boldsymbol{v}-\bar{\boldsymbol{u}})d\Gamma - \frac{1}{2m}\int_{\Omega_\Gamma}\boldsymbol{E}:(\boldsymbol{\varepsilon}(\boldsymbol{\zeta})-\boldsymbol{\varepsilon}(\boldsymbol{u}))^2 d\Omega$
$\Pi_{ib/stp/fat}$	$\Pi(\boldsymbol{v})$
$\Pi(\boldsymbol{v})$	$\int_\Omega v_\varepsilon(\boldsymbol{v})d\Omega - \int_\Omega \boldsymbol{v}\cdot\boldsymbol{b}d\Omega - \int_{\Gamma_N}\boldsymbol{v}\cdot\bar{\boldsymbol{g}}d\Gamma$
$\Pi^*(\boldsymbol{v},\boldsymbol{\zeta})$	$\int_\Omega v^*_\varepsilon(\boldsymbol{v},\boldsymbol{\zeta})d\Omega - \int_\Omega \boldsymbol{v}\cdot\boldsymbol{b}d\Omega - \int_{\Gamma_N}\boldsymbol{v}\cdot\bar{\boldsymbol{g}}d\Gamma$

Table 2: Solution systems of equations

functional	solution system
$\Pi_L(\boldsymbol{v},\boldsymbol{\gamma})$	$\begin{bmatrix}\boldsymbol{K} & \boldsymbol{G}\\ \boldsymbol{G}^T & \boldsymbol{0}\end{bmatrix}\begin{Bmatrix}\boldsymbol{u}^e\\ \boldsymbol{\lambda}^e\end{Bmatrix} = \begin{Bmatrix}\boldsymbol{f}\\ \boldsymbol{f}_L\end{Bmatrix}$
$\Pi_{pen}(\boldsymbol{v})$	$(\boldsymbol{K}+\boldsymbol{K}_p)\boldsymbol{u}^e = \boldsymbol{f}+\boldsymbol{f}_p$
$\Pi_{Nit}(\boldsymbol{v})$	$[\boldsymbol{K}+\boldsymbol{K}_p-(\boldsymbol{K}_N+\boldsymbol{K}_N^T)]\boldsymbol{u}^e = \boldsymbol{f}+\boldsymbol{f}_p-\boldsymbol{f}_N$
$\Pi_{H-R}(\boldsymbol{v},\boldsymbol{\zeta})$	$\begin{bmatrix}\boldsymbol{0} & \boldsymbol{A}_s\\ \boldsymbol{A}_s^T & -\boldsymbol{K}_s\end{bmatrix}\begin{Bmatrix}\boldsymbol{u}^e\\ \boldsymbol{\sigma}^e\end{Bmatrix} = \begin{Bmatrix}\boldsymbol{f}\\ -\boldsymbol{f}_s\end{Bmatrix}$, $\Rightarrow \boldsymbol{A}_s^T\boldsymbol{u}^e = \boldsymbol{K}_s\boldsymbol{A}_s^{-1}\boldsymbol{f}-\boldsymbol{f}_s$
$\Pi_{LLM}(\boldsymbol{v},\boldsymbol{\zeta})$	$\begin{bmatrix}\boldsymbol{K}-\boldsymbol{K}_\Gamma & \boldsymbol{A}_{s2}\\ \boldsymbol{A}_{s2}^T & -\boldsymbol{K}_{s2}\end{bmatrix}\begin{Bmatrix}\boldsymbol{u}^e\\ \boldsymbol{\sigma}^e\end{Bmatrix} = \begin{Bmatrix}\boldsymbol{f}\\ -\boldsymbol{f}_s\end{Bmatrix}$ $\Rightarrow (\boldsymbol{K}-\boldsymbol{K}_\Gamma+\boldsymbol{A}_{s2}\boldsymbol{K}_{s2}^{-1}\boldsymbol{A}_{s2}^T)\boldsymbol{u}^e = \boldsymbol{f}-\boldsymbol{A}_{s2}\boldsymbol{K}_{s2}^{-1}\boldsymbol{f}_s$
$\Pi_{ib}=\Pi(\boldsymbol{v})$	$\hat{\boldsymbol{K}}\boldsymbol{u}_g^e = \hat{\boldsymbol{f}}-\boldsymbol{f}_{ib}$
$\Pi_{stp}=\Pi(\boldsymbol{v})$	$(\boldsymbol{K}+\boldsymbol{K}_{stp})\boldsymbol{u}^e = \boldsymbol{f}-\boldsymbol{f}_{stp}$
$\Pi_{fat}=\Pi(\boldsymbol{v})$	$\begin{cases}\boldsymbol{K}_{(a)}\boldsymbol{d}^e = \boldsymbol{f}_{(a)}\\ \boldsymbol{K}_{(b)}\hat{\boldsymbol{u}}^e = \boldsymbol{f}_{(b)}+\boldsymbol{f}_{at}\end{cases}$

section, we propose methods that impose inclined and partially prescribed boundary conditions in

a common format with most of these methods.

We start with the energy functionals from the previous section to give clear physical interpretations to the modifications. In order to impose different conditions in orthogonal directions along a boundary, the additional boundary condition integrals in the energy functionals introduced in the preceding section should be treated locally, i.e. the contribution of each direction to these boundary integrals should be computed separately. Recalling the notation used in (1), where local coordinates x_i' $(i = 1, 2)$ are defined to be aligned with the two orthogonal directions and $\boldsymbol{\alpha}$ is the transformation tensor, the coordinate transformation for a global vector v_i $(i = 1, 2)$ can be expressed as $\boldsymbol{v}' = \boldsymbol{\alpha} \cdot \boldsymbol{v}$ (where $(\cdot)'$ indicates local quantities). A local indicator $\boldsymbol{\psi}'$ is defined as

$$\psi_i' = \begin{cases} 1, & u_i' = \bar{u}_i', \\ 0, & u_i' \text{ unconstrained}, \end{cases} \qquad i = 1, 2, \tag{87}$$

to describe the boundary condition applied to a certain boundary, such that when local quantities (e.g. the locally penalised displacement in the penalty method) are weighted by the indicator, any influence of the boundary condition in an unconstrained direction is removed (for example in the case of a roller boundary condition). The following formulations generalise to fully prescribed Dirichlet boundaries Γ_D with $\psi_1' = \psi_2' = 1$.

Lagrange multiplier method. Lagrange multipliers $\boldsymbol{\gamma}$ in the energy functional (10) are physically interpreted as the traction unknowns along the Dirichlet boundary, which are non-zero only in directions where the displacement is prescribed. By using the local indicator $\boldsymbol{\psi}'$ to weight the transformed tractions $\boldsymbol{\alpha} \cdot \boldsymbol{\gamma}$, the local traction unknown becomes

$$\boldsymbol{\gamma}' = \boldsymbol{\psi}' \cdot \boldsymbol{\delta} \cdot \boldsymbol{\alpha} \cdot \boldsymbol{\gamma}, \tag{88}$$

where $\boldsymbol{\delta}$ is the Kronecker delta. This local quantity is then transformed back into global coordinates, i.e. (88) is dotted by $\boldsymbol{\alpha}^{-1} = \boldsymbol{\alpha}^T$ on the left, giving the modified energy functional as

$$\Pi_L(\boldsymbol{v}, \boldsymbol{\gamma}) = \Pi(\boldsymbol{v}) + \int_{\Gamma_D \cup \Gamma_T} \bar{\boldsymbol{\psi}} \cdot \boldsymbol{\gamma} \cdot (\boldsymbol{v} - \bar{\boldsymbol{u}}) d\Gamma, \tag{89}$$

where $\bar{\boldsymbol{\psi}} = \boldsymbol{\alpha}^T \cdot \boldsymbol{\psi}' \cdot \boldsymbol{\delta} \cdot \boldsymbol{\alpha}$. Matrix notations of the local tensor $\boldsymbol{\psi}' \cdot \boldsymbol{\delta}$ and the transformation tensor $\boldsymbol{\alpha}$ are

$$\boldsymbol{\varphi}' = \begin{bmatrix} \psi_1' & 0 \\ 0 & \psi_2' \end{bmatrix} \qquad \text{and} \qquad \boldsymbol{T} = \begin{bmatrix} \cos t & \sin t \\ -\sin t & \cos t \end{bmatrix}, \tag{90}$$

where t denotes the rotation angle from $\boldsymbol{x}$ to $\boldsymbol{x}_1'$, such that the modified matrices in the final system of equations become

$$\boldsymbol{G} = \int_{\Gamma^e_{D/T}} \boldsymbol{N}^T \bar{\boldsymbol{\varphi}} \boldsymbol{N}_L d\Gamma \qquad \text{and} \qquad \boldsymbol{f}_L = \int_{\Gamma^e_{D/T}} \boldsymbol{N}_L^T \bar{\boldsymbol{\varphi}} \bar{\boldsymbol{u}} d\Gamma, \tag{91}$$

where $\bar{\boldsymbol{\varphi}} = \boldsymbol{T}^T \boldsymbol{\varphi}' \boldsymbol{T}$.

Penalty method. The additional term of the penalty method in functional (17) should only influence the constrained local directions. In order to cancel the penalised displacement and boundary value in directions where correspondent conditions are "unconstrained", the indicator $\boldsymbol{\psi}'$ is used to weight

$\boldsymbol{\alpha}\cdot(\boldsymbol{v}-\bar{\boldsymbol{u}})$, such that the difference between the local displacement and the boundary value becomes

$$\boldsymbol{v}' - \bar{\boldsymbol{u}}' = \boldsymbol{\psi}' \cdot \boldsymbol{\delta} \cdot \boldsymbol{\alpha} \cdot (\boldsymbol{v} - \bar{\boldsymbol{u}}). \tag{92}$$

Transforming this quantity back to global coordinates with $\boldsymbol{\alpha}^{-1} = \boldsymbol{\alpha}^T$ gives the modified energy functional

$$\Pi_{pen}(\boldsymbol{v}) = \Pi(\boldsymbol{v}) + \frac{\beta}{2} \int_{\Gamma_D \cup \Gamma_T} \bar{\boldsymbol{\psi}} \cdot (\boldsymbol{v} - \bar{\boldsymbol{u}})^2 d\Gamma, \tag{93}$$

leading to the following modified matrices in the final system

$$\boldsymbol{K}_p = \beta \int_{\Gamma^e_{D/T}} \boldsymbol{N}^T \bar{\boldsymbol{\varphi}} \boldsymbol{N} d\Gamma \qquad \text{and} \qquad \boldsymbol{f}_p = \beta \int_{\Gamma^e_{D/T}} \boldsymbol{N}^T \bar{\boldsymbol{\varphi}} \bar{\boldsymbol{u}} d\Gamma. \tag{94}$$

Nitsche's method. The penalty term in Nitsche's method (the last integral in (26)) is treated the same way as in (93). The first additional integral in the functional (26) has the form of the product of the traction $-\boldsymbol{\sigma}(\boldsymbol{v}) \cdot \boldsymbol{n}$ and the displacement $\boldsymbol{v}$, whereby analogy can be made to that in the Lagrange multiplier method: (88) and (89), where tractions are transformed to local coordinates, weighted separately and transformed back again. The energy functional of Nitsche's method therefore becomes

$$\Pi_{Nit}(\boldsymbol{v}) = \Pi(\boldsymbol{v}) - \int_{\Gamma_D \cup \Gamma_T} \bar{\boldsymbol{\psi}} \cdot \boldsymbol{\sigma}(\boldsymbol{v}) \cdot \boldsymbol{n} \cdot (\boldsymbol{v} - \bar{\boldsymbol{u}}) d\Gamma + \frac{\beta}{2} \int_{\Gamma_D \cup \Gamma_T} \bar{\boldsymbol{\psi}} \cdot (\boldsymbol{v} - \bar{\boldsymbol{u}})^2 d\Gamma, \tag{95}$$

which leads to, besides (94), the following modified matrices in the final system

$$\boldsymbol{K}_N = \int_{\Gamma^e_{D/T}} \boldsymbol{B}^T \boldsymbol{D} \hat{\boldsymbol{n}}^T \bar{\boldsymbol{\varphi}} \boldsymbol{N} d\Gamma \qquad \text{and} \qquad \boldsymbol{f}_N = \int_{\Gamma^e_{D/T}} \boldsymbol{B}^T \boldsymbol{D} \hat{\boldsymbol{n}}^T \bar{\boldsymbol{\varphi}} \bar{\boldsymbol{u}} d\Gamma. \tag{96}$$

LLM (symmetric). The first additional term in functional (55) introduces the stress field as Lagrange multipliers, such that it is modified in a way analogous to (88) and (89), while the other additional term in (55), which links the two unknown fields weakly near the Dirichlet boundary, remains unchanged. The energy functional of the LLM method becomes

$$\Pi_{LLM}(\boldsymbol{v}, \boldsymbol{\zeta}) = \Pi(\boldsymbol{v}) - \int_{\Gamma_D \cup \Gamma_T} \bar{\boldsymbol{\psi}} \cdot \boldsymbol{\zeta} \cdot \boldsymbol{n} \cdot (\boldsymbol{v} - \bar{\boldsymbol{u}}) d\Gamma - \frac{1}{2m} \int_{\Omega_\Gamma} \boldsymbol{E} : (\boldsymbol{\varepsilon}(\boldsymbol{\zeta}) - \boldsymbol{\varepsilon}(\boldsymbol{v}))^2 d\Omega, \tag{97}$$

leading to the following modified system

$$\boldsymbol{G}_s = \int_{\Gamma^e_{D/T}} \boldsymbol{N}^T \bar{\boldsymbol{\varphi}} \hat{\boldsymbol{n}} \boldsymbol{N}_s d\Gamma \qquad \text{and} \qquad \boldsymbol{f}_s = \int_{\Gamma^e_{D/T}} \boldsymbol{N}_s^T \hat{\boldsymbol{n}}^T \bar{\boldsymbol{\varphi}} \bar{\boldsymbol{u}} d\Gamma, \tag{98}$$

while the rest of the matrices in the system remain unchanged.

The stress field is condensed at the element level, which gives rise to the inverse operation of $\boldsymbol{K}_{s2}$ as is shown in (61). However, $\boldsymbol{K}_{s2}$ is often close to singular and the inverse $\boldsymbol{K}_{s2}^{-1}$ gives elements with enormous values. It barely affect the result on fully fixed Dirichlet boundaries, but locking has been observed when it comes to inclined roller boundaries as the large values act as penalty parameters that restraint the boundaries from moving. In the implementation, the Moore-Penrose pseudo inverse [58], $\boldsymbol{K}_{s2}^{+}$, is calculated instead of the direct inverse, which gives good performance, i.e.

$$(\boldsymbol{K} - \boldsymbol{K}_\Gamma + \boldsymbol{A}_{s2} \boldsymbol{K}_{s2}^{+} \boldsymbol{A}_{s2}^T) \boldsymbol{u}^e = \boldsymbol{f} + \boldsymbol{A}_{s2} \boldsymbol{K}_{s2}^{+} \boldsymbol{f}_s. \tag{99}$$

Step boundary method. The application of the step boundary method to the inclined Dirichlet boundary starts with local Dirichlet functions ω_i' $(i = 1, 2)$ (which equal to either unity or $\omega(\phi)$ as described in Section 3.2.1), which are employed in the local displacement unknowns as

$$\boldsymbol{u}' = \boldsymbol{\omega}' \cdot \boldsymbol{\delta} \cdot \boldsymbol{u}_g' + \boldsymbol{u}_a'. \tag{100}$$

Applying coordinate transformation to (100) between global and local coordinates gives

$$\boldsymbol{u} = \bar{\boldsymbol{\omega}} \cdot \boldsymbol{u}_g + \boldsymbol{u}_a, \tag{101}$$

where $\bar{\boldsymbol{\omega}} = \boldsymbol{\alpha}^T \cdot \boldsymbol{\omega}' \cdot \boldsymbol{\delta} \cdot \boldsymbol{\alpha}$, based on which the finite element formulation can be derived. For more details of the derivation, the reader is referred to [47].

Fat boundary method. To impose the inclined and partially prescribed boundary in the fat boundary method, the transformation technique should be employed in the local crust-like mesh the same way as in the classical finite element method [59].

5. Numerical examples

This section aims to discover how the algorithmic parameters in formulations of the penalty method, Nitsche's method, the symmetric LLM method and the step boundary method affect their performance. Elastic problems with plane stress conditions are assumed in all examples. Square background elements with side length h are used with linear isotropic elastic material (with Young's modulus $E = 1$kPa and and Poisson's ratio $\nu = 0.3$). The performance of the approaches is assessed using error measures based on analytical solutions. Relative errors in $\mathscr{L}^2$ and energy norms for displacement and stress results are respectively defined as

$$e_u = \frac{||\boldsymbol{u}^h - \boldsymbol{u}^a||_{\mathscr{L}^2(\Omega)}}{||\boldsymbol{u}^a||_{\mathscr{L}^2(\Omega)}} = \sqrt{\frac{\int_\Omega ||\boldsymbol{u}^h - \boldsymbol{u}^a||^2 d\Omega}{\int_\Omega ||\boldsymbol{u}^a||^2 d\Omega}} \tag{102}$$

and

$$e_\sigma = \frac{||\boldsymbol{u}^h - \boldsymbol{u}^a||_{\mathscr{E}(\Omega)}}{||\boldsymbol{u}^a||_{\mathscr{E}(\Omega)}} = \sqrt{\frac{\int_\Omega (\boldsymbol{\varepsilon}^h - \boldsymbol{\varepsilon}^a) : (\boldsymbol{\sigma}^h - \boldsymbol{\sigma}^a) d\Omega}{\int_\Omega \boldsymbol{\varepsilon}^a : \boldsymbol{\sigma}^a d\Omega}}, \tag{103}$$

where superscripts $(\cdot)^h$ and $(\cdot)^a$ denote the finite element and analytical solutions, respectively.

5.1. Circular cavity expansion

The first example is the axi-symmetric expansion of a cavity with internal and external radii $r_1 = 0.5$m and $r_2 = 1$m respectively, subjected to internal pressure $p = 0.1$kPa. One-eighth of the cavity is modelled with roller boundary conditions and using linear elements, as shown in Figure 5. Through this example, we investigate the choices of algorithmic parameters as well as the behaviour of inclined roller boundaries imposed using different methods.

Figure 6 shows absolute errors of displacement and von Mises stress obtained with $h = 0.0625$m in contour plots for the LLM method. Errors are larger at the internal boundary at which pressure is imposed than at the outer edge. Relatively large errors are measured where only a small fraction of an element is integrated. The displayed error contours were obtained with roller boundary conditions being imposed using Nitsche's method, with $\beta = 10^5$ and similar distributions of errors

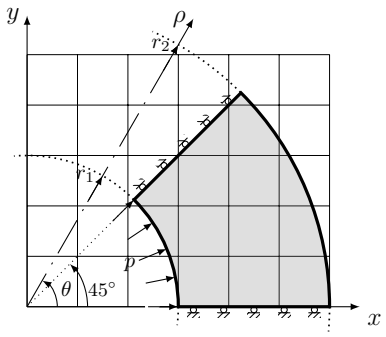

Figure 5: Problem setting of the circular cavity expansion problem with roller boundaries and coordinate systems.

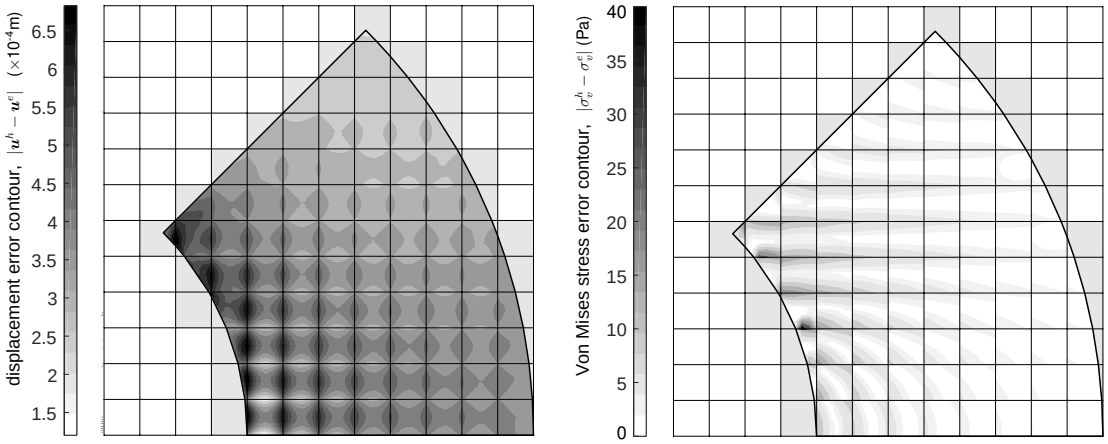

Figure 6: Error contours obtained with Nitsche's method ($\beta = 10^5$, $h = 0.0625$m) for the circular cavity expansion problem.

are obtained with the other three methods, as long as their parameters β, m and ϵ are appropriately chosen.

We now test the sensitivity of methods to variation in the respective algorithmic parameters β, m and ϵ^{-1}, each varying from 0.1 to 10^{20}. Displacement errors obtained with a grid of $h = 0.125$m are plotted in Figure 7. With increasing values of the parameters, errors of all these methods converge to a stage where the finite element discretisation becomes the predominant factor that decides the accuracy of calculations, and at this stage, the accuracy of these methods is not distinguishable. In the succeeding text, this stage is referred to as a "plateau", followed by the divergence at the right hand end of the plot which results from ill-conditioning of the global stiffness matrices.

The minimum errors of two penalty methods, the original penalty method and the step boundary method, do not appear at the plateau because of the mismatch between the analytical and discretised solutions (recalling that these errors are calculated for a given fixed discretisation). The inset plot in Figure 7 shows that the absolute displacements of these two methods go through the analytical value and then converge monotonically. Error patterns of these two methods are observed to be similar, which simply improves with the growth in β and ϵ^{-1} until the error of the domain discretisation dominates. The distance between these two curves indicates that the

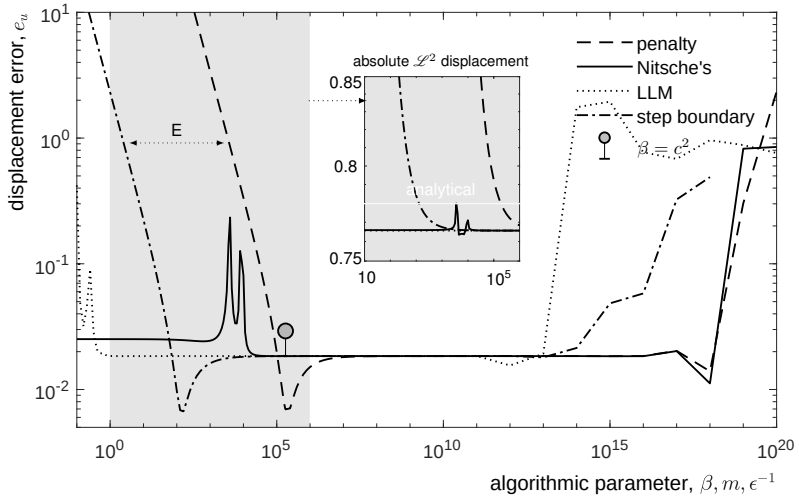

Figure 7: Displacement errors against algorithmic parameters for the circular cavity expansion problem with $h = 0.125$m; inset plot: $||\boldsymbol{u}^h||_{\mathscr{L}^2(\Omega)}$ and $||\boldsymbol{u}^a||_{\mathscr{L}^2(\Omega)}$ (the white line) against parameters.

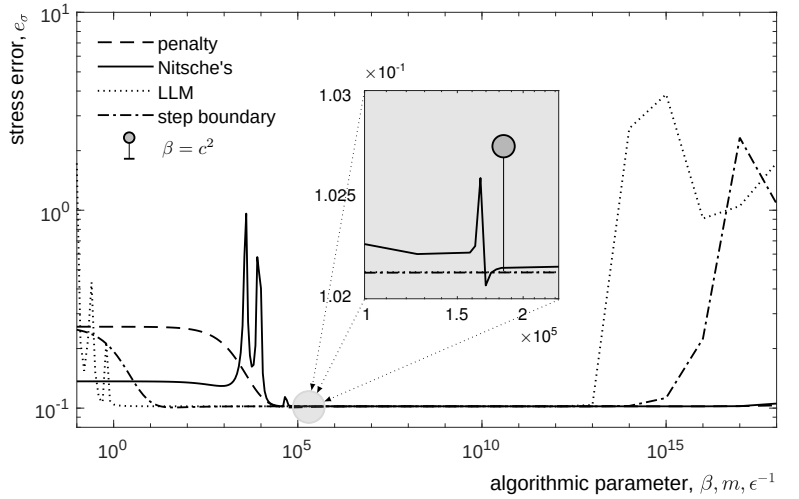

Figure 8: Stress errors against algorithmic parameters for the circular cavity expansion problem with $h = 0.125$m.

magnitude of the penalty factor in the step boundary method is of the same order as E/ϵ. For the LLM method, the performance is not sensitive for all $m > 1$, which justifies the stability condition. Similar conclusions can be drawn from observation of stress errors in Figure 8.

The errors of Nitsche's method fluctuate at a certain stage, suggesting instability with respect to β. The error hits the plateau within a small distance from the unstable section, and there are some slight fluctuations after that, easier to see in the stress error. The range of β where fluctuations appear depends on both the finite element discretisation and the scheme for the boundary integrals, and can be estimated through the eigenvalue problem (39). In a series of calculations, it is observed

that the largest eigenvalue c^2 always gives a safe β that often lies right after the last peak of the detected fluctuations (shown in the inset plot of Figure 8 for this case), which ensures stability.

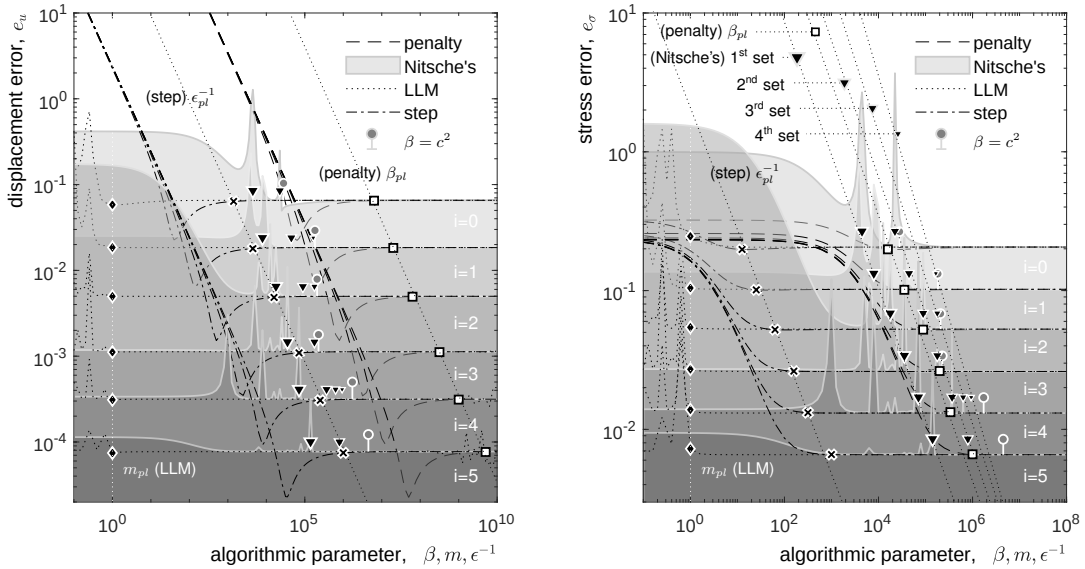

Figure 9: Errors against algorithmic parameters with uniform grid refinement. Results for the circular cavity expansion problem.

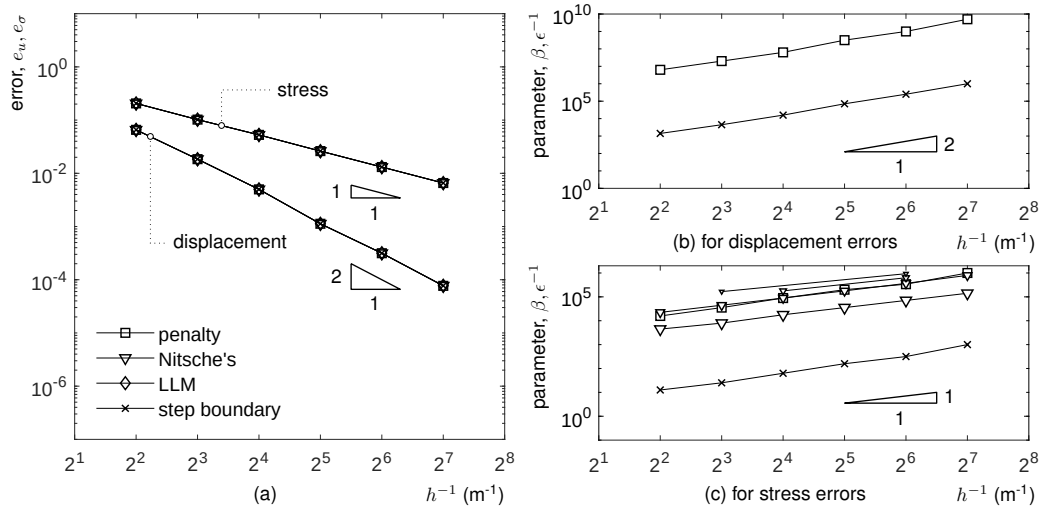

Figure 10: Circular cavity expansion: (a) convergence of displacement and stress errors obtained with $\beta = 10^{10}$, $m = 1$ and $\epsilon = 10^{-7}$, (b) critical parameters for displacement errors against refinement and (c) critical parameters for stress errors against refinement

To study convergence with h-refinement, an initial coarse grid with $h_0 = 0.25$ is uniformly

refined, with the element size h being halved each time, such that $h = h_0 \times 2^{-i}$ after the ith refinement. The errors are plotted against the algorithmic parameters and the grid refinement in Figure 9.

As long as the algorithmic parameter of each method is chosen from the plateau, i.e. where the finite element discretisation error predominates, the same optimal convergence as the classical finite element method can be achieved. Logarithmic rates of convergence in $\mathscr{L}^2$ and energy norms are shown in Figure 10(a), and gradients approximate to 2 and 1 are observed for displacement and stress errors, respectively, with appropriately chosen parameters (both $\beta = 10^{10}$, $m = 1$ and $\epsilon = 10^{-7}$), which agrees with the theoretical convergence rate of the finite element method ($p+1$ in terms of the displacement convergence rate, for example). However, the plateaus of some methods move rightwards with grid refinement, as discussed below.

In the LLM method, any $m > 1$ ensures stability and this condition does not depend on the grid size, as verified for this example in Figure 9. Errors strike the plateau shortly after $m = 1$, such that optimal convergence is obtained in both $\mathscr{L}^2$ and energy norms for the simple choice of $m_{pl} = 1$, marked with diamonds in Figure 9.

In the fluctuating sections of Nitsche's method in Figure 9, the peaks rise in sets. For each grid size, peaks appear at same values of β in both $\mathscr{L}^2$ and energy norms. We labelled four set of peaks which appear in rightmost positions in the energy norm in Figure 9, each set being marked with triangles. For most grid sizes, errors strike the plateaus shortly after the first set, and the amplitudes of the rest shrink with the growth in β. For a certain grid size, peaks are not necessarily captured for all these sets; they either do not exist or are too narrow to be captured. These sets generally move in proportion to h^{-1} in respect of β , as shown in Figure 10(c), marked with triangles of different sizes which correspond to those in Figure 9. This indicates that optimal rates of convergence can be achieved both in $\mathscr{L}^2$ and energy norms if β is taken to be the order of h^{-1}, providing $\beta|_{i=0}$ is chosen within the plateau, which agrees with the stability condition (34).

The penalty method does not need stabilisation, so we take $\beta = \beta_{pl}$, marked with squares, with the subscript $(\cdot)_{pl}$ denoting where the error is close enough to the start of the plateau, to quantify the movement of the plateau with respect to h. These critical β_{pl} for the penalty method are plotted against refinement using square markers in Figure 10(b) and (c), which illustrate the increase of β_{pl} proportional to h^{-2} in the $\mathscr{L}^2$ norm and h^{-1} in the energy norm, respectively. The results agree with convergence condition (25) of $\beta = \eta h^{-(2p+1)/3}$ in the energy norm, with $p = 1$. The results also show the lack of optimality in the $\mathscr{L}^2$ norm for the same choice of β. Compared to the condition for Nitsche's method, β in penalty methods would be much greater for a fine grid and higher order elements, which is more likely to lead to ill-conditioning. The step boundary method behaves similarly, which is illustrated by the plots of ϵ_{pl} against refinement in Figure 10(b) and (c).

5.2. Tension in a perforated infinite plate

The second example is an infinite plate with a circular hole of radius $r = 0.5$m in the centre, subjected to uni-directional in-plane tension of $p = 0.1$kPa. We model both a 60° portion and a quadrant here with $l = 1$m, as shown in Figure 11, using linear elements. Apart from the homogeneous Neumann boundary at $\rho = r$, we prescribe displacement on the other four boundaries to investigate the performance of the imposition methods for non-uniform inhomogeneous Dirichlet boundaries. The analytical solution for the displacement field is given as [60]

$$u_x(\rho,\theta) = \frac{1+\nu}{E} p \left(\frac{\rho}{1+\nu}\cos\theta + \frac{2r^2}{(1+\nu)\rho}\cos\theta + \frac{r^2}{2\rho}\cos 3\theta - \frac{r^4}{2\rho^3}\cos 3\theta \right) \tag{104}$$

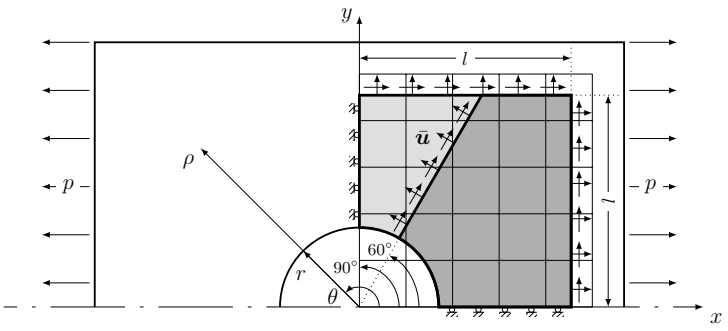

Figure 11: Half perforated infinite plate and problem setting for models of: (a) a quadrant (the entire grey area) and (b) a 60° portion (the area filled with dark grey), and coordinate systems.

and

$$u_y(\rho,\theta) = \frac{1+\nu}{E}p\left(\frac{-\nu\rho}{1+\nu}\sin\theta - \frac{(1-\nu)r^2}{(1+\nu)\rho}\sin\theta + \frac{r^2}{2\rho}\sin 3\theta - \frac{r^4}{2\rho^3}\sin 3\theta\right). \tag{105}$$

The results of parametric and convergence studies are displayed for both models, with the initial grid $h_0 = 0.3$m being uniformly refined such that $h = 0.3 \times 2^{-i}$m after the ith refinement.

5.2.1. Model of a quadrant

In the quadrant model, boundaries at $x = 0$ and $y = 0$ in the quadrant model are set as rollers due to symmetry, and boundaries at $x = l$ and $y = l$ are inhomogeneous Dirichlet boundaries, fully prescribed in accordance with the analytical solutions of displacement.

Figure 12 shows contours of absolute errors obtained with $h = 0.075$m. The displayed result is obtained with Dirichlet boundary conditions being imposed using the step boundary method with $\epsilon = 10^{-5}$. Similar distributions of errors are obtained with the other three methods with appropriate parameters. Large values of both displacement and stress errors are measured near the free boundary.

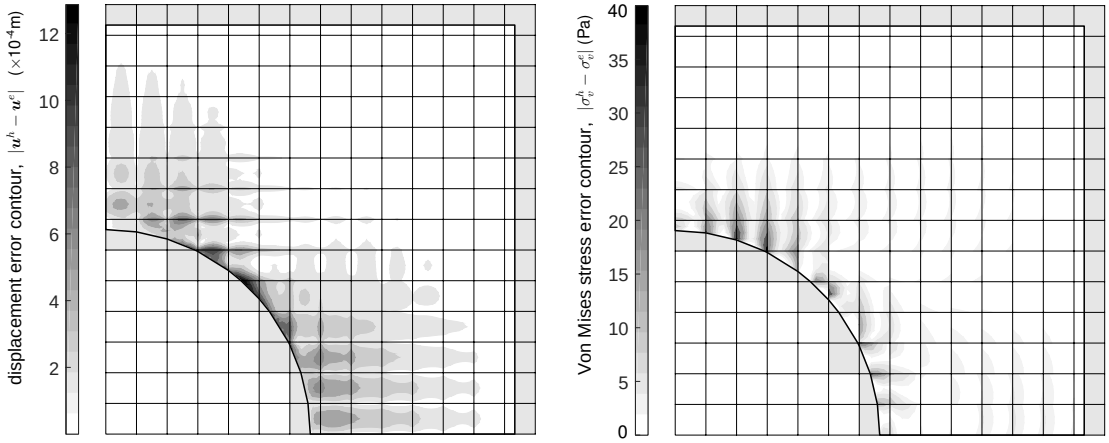

Figure 12: Error contours obtained with the step boundary method ($\epsilon = 10^{-5}$, $h = 0.075$m) for the quadrant plate.

Displacement and stress errors are plotted against the algorithmic parameters in Figure 13. Error patterns similar to the first example are observed for all four methods. In Figure 14(a),

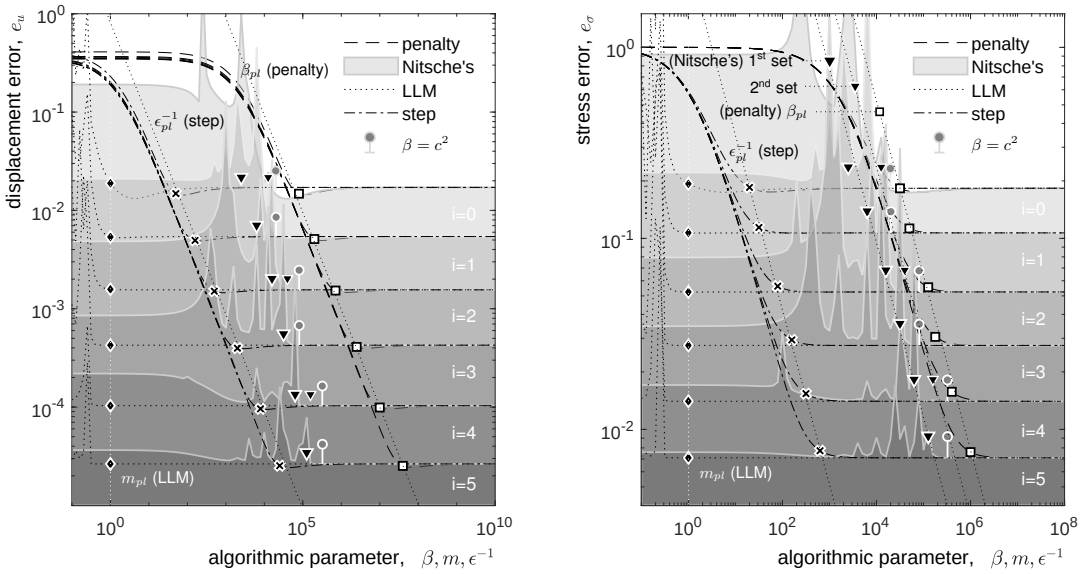

Figure 13: Errors against algorithmic parameters with uniform grid refinement. Results for the quadrant plate.

displacement and stress error plots show optimal rates of convergence (calculated with both $\beta = 10^8$, $m = 1$ and $\epsilon = 10^{-5}$), and Figure 14(b) and (c) show the movement of plateaus with grid refinement in $\mathscr{L}^2$ and energy norms, respectively. The same conclusions as the first example on the choice of parameters with regard to the grid size can be drawn.

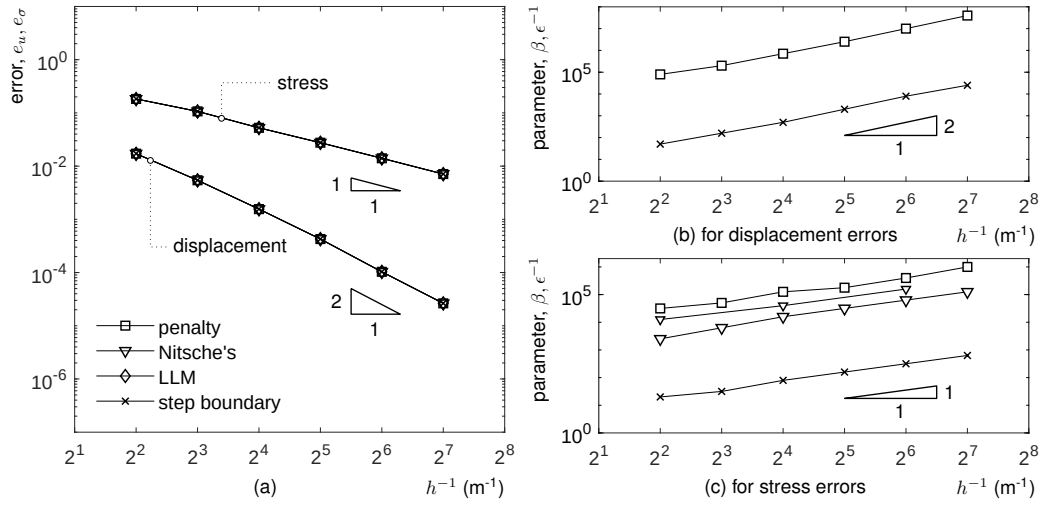

Figure 14: Quadrant plate: (a) convergence of displacement and stress errors obtained with $\beta = 10^8$, $m = 1$ and $\epsilon = 10^{-5}$, (b) critical parameters for displacement errors against refinement and (c) critical parameters for stress errors against refinement

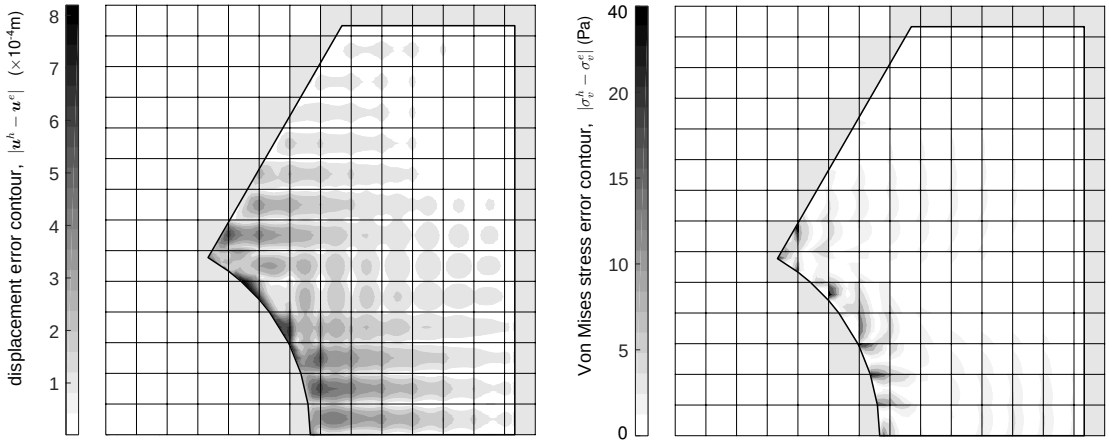

Figure 15: Error contours obtained with the LLM method ($m = 1$, $h = 0.075$m) for the 60° plate.

5.2.2. Model of a 60° portion

In this model, the boundary at $y = 0$ in the 60° model are set as a roller, and the other boundaries as inhomogeneous Dirichlet boundaries apart from the free boundary at $\rho = r$. This example demonstrates the feature of the non-uniform displacement being prescribed to an inclined boundary.

Figure 15 shows the solution of displacement and stress errors in contour plots obtained with $h = 0.075$m. The displayed result is obtained with Dirichlet boundary conditions being imposed using the LLM method with $m = 1$. The errors are plotted against the algorithmic parameters in Figure 16. For inclined boundaries with non-uniform Dirichlet boundary conditions, the displacement is clearly more sensitive to the parameters, especially with relatively coarse grids ($i = 0, 1$), but generally, we are able to find similar error patterns with respect to the parameters for all methods after the second grid refinement.

The eigenvalue estimations for Nitsche's parameter often lie close to where displacement errors in the penalty method hit plateaus, which is clear to observe in this example in which the signs of displacement error do not flip. This is due to the fact that the action of the boundary integral added for consistency in Nitsche's method is weakened during numerical integration.

Similar to previous examples, Figure 17 shows optimal convergence and the moving rates of plateaus with respect to grid refinement in both $\mathscr{L}^2$ and energy norms. The obtained optimal convergence is calculated with $\beta = 10^8$, $m = 1$ and $\epsilon = 10^{-5}$.

Conclusions

Weak imposition methods allow Dirichlet boundary conditions to be imposed in fictitious domain based approaches. In this article, we have reviewed the Hellinger-Reissner principle, the LLM method, the implicit boundary method and the fat boundary method along with the well-known Lagrange multiplier, penalty and Nitsche's methods, derived and compared them starting with energy functionals and weak forms, and formulated the systems of equations using the fictitious domain finite element method. A selection of these methods have then been extended to partially prescribed boundaries with inclination for the first time here, followed by presentation of numerical example as validations. The parametric choices in the penalty, LLM, step boundary and Nitsche's

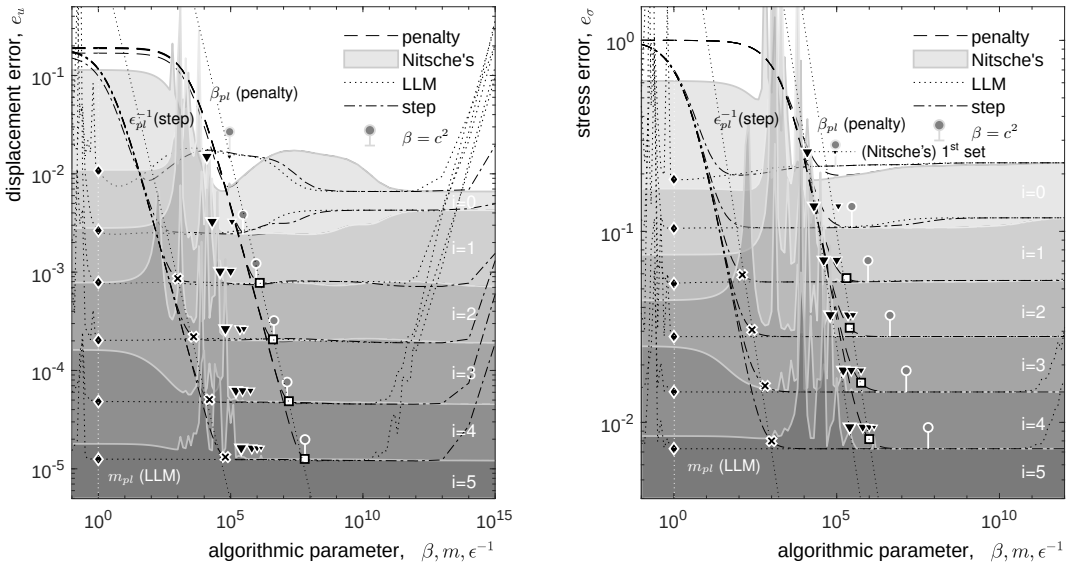

Figure 16: Errors against algorithmic parameters with uniform grid refinement. Results for the 60° plate.

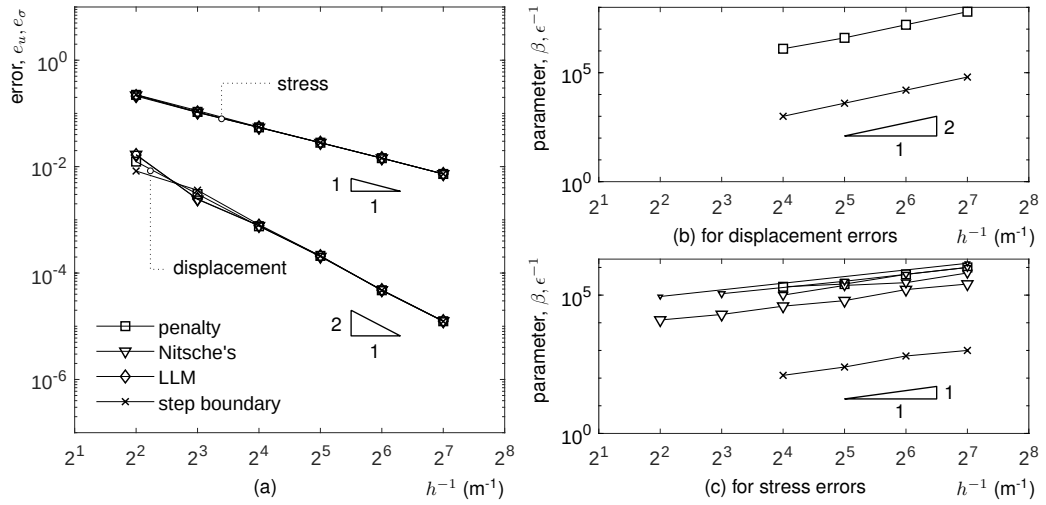

Figure 17: 60° plate: (a) convergence of displacement and stress errors obtained with $\beta = 10^8$, $m = 1$ and $\epsilon = 10^{-5}$, (b) critical parameters for displacement errors against refinement and (c) critical parameters for stress errors against refinement

methods, which contain algorithmic parameters, are discussed through numerical examples. We observed the existence of "plateaus" in error plots of these methods against their parameters, and have demonstrated movement of these plateaus moves with grid refinement at a certain rate, which has been linked to previous convergence theories. We have also demonstrated optimal rates of convergence using these methods, as long as the parameters are chosen within the plateaus.

Acknowledgements

The authors gratefully acknowledge the financial support from the China Scholarship Council.

[1] C. S. Peskin, Flow patterns around heart valves: a numerical method, Journal of computational physics 10 (2) (1972) 252–271.
[2] C. S. Peskin, The immersed boundary method, Acta Numerica 11.
[3] R. Glowinski, T.-W. Pan, J. Periaux, A fictitious domain method for Dirichlet problem and applications, Computer Methods in Applied Mechanics and Engineering 111 (3-4) (1994) 283–303.
[4] H. Johansen, P. Colella, A Cartesian grid embedded boundary method for Poisson's equation on irregular domains, Journal of Computational Physics 147 (1) (1998) 60–85.
[5] A. V. Kumar, S. Padmanabhan, R. Burla, Implicit boundary method for finite element analysis using non-conforming mesh or grid, International Journal for Numerical Methods in Engineering 74 (9) (2008) 1421–1447.
[6] A. C. Ramos, A. M. Aragón, S. Soghrati, P. H. Geubelle, J.-F. Molinari, A new formulation for imposing Dirichlet boundary conditions on non-matching meshes, International Journal for Numerical Methods in Engineering 103 (6) (2015) 430–444.
[7] L. Quiroz, P. Beckers, Non-conforming mesh gluing in the finite elements method, International Journal for Numerical Methods in Engineering 38 (13) (1995) 2165–2184.
[8] R. Becker, P. Hansbo, R. Stenberg, A finite element method for domain decomposition with non-matching grids, ESAIM: Mathematical Modelling and Numerical Analysis 37 (2) (2003) 209–225.
[9] I. Babuška, The finite element method with Lagrangian multipliers, Numerische Mathematik 20 (3) (1973) 179–192.
[10] I. Babuška, The finite element method with penalty, Mathematics of computation 27 (122) (1973) 221–228.
[11] J. Nitsche, Über ein variationsprinzip zur lösung von Dirichlet-problemen bei verwendung von teilräumen, die keinen randbedingungen unterworfen sind, in: Abhandlungen aus dem mathematischen Seminar der Universität Hamburg, Vol. 36, Springer, Elsevier, 1971, pp. 9–15.
[12] J. Baiges, R. Codina, F. Henke, S. Shahmiri, W. A. Wall, A symmetric method for weakly imposing Dirichlet boundary conditions in embedded finite element meshes, International Journal for Numerical Methods in Engineering 90 (5) (2012) 636–658.
[13] J.-H. He, Generalized Hellinger-Reissner principle, Journal of applied mechanics 67 (2) (2000) 326–331.
[14] B. Maury, A fat boundary method for the Poisson problem in a domain with holes, Journal of scientific computing 16 (3) (2001) 319–339.
[15] S. Fernández-Méndez, A. Huerta, Imposing essential boundary conditions in mesh-free methods, Computer methods in applied mechanics and engineering 193 (12) (2004) 1257–1275.
[16] W. Zhang, L. Zhao, Exact imposition of inhomogeneous Dirichlet boundary conditions based on weighted finite cell method and level-set function, Computer Methods in Applied Mechanics and Engineering 307 (2016) 316–338.
[17] R. Stenberg, On some techniques for approximating boundary conditions in the finite element method, Journal of Computational and applied Mathematics 63 (1-3) (1995) 139–148.
[18] D. N. Arnold, F. Brezzi, B. Cockburn, L. D. Marini, Unified analysis of discontinuous Galerkin methods for elliptic problems, SIAM journal on numerical analysis 39 (5) (2002) 1749–1779.
[19] J. Parvizian, A. Düster, E. Rank, Finite cell method, Computational Mechanics 41 (1) (2007) 121–133.
[20] K. Höllig, U. Reif, J. Wipper, Weighted extended B-spline approximation of Dirichlet problems, SIAM Journal on Numerical Analysis 39 (2) (2001) 442–462.
[21] L. V. Kantorovich, V. I. Krylov, C. D. Benster, G. Weiss, Approximate methods of higher analysis, Physics Today 13 (1) (1960) 74–76.
[22] M. A. Yerry, M. S. Shephard, A modified quadtree approach to finite element mesh generation, IEEE Computer Graphics and Applications 3 (1) (1983) 39–46.
[23] Y. Lu, T. Belytschko, L. Gu, A new implementation of the element free Galerkin method, Computer methods in applied mechanics and engineering 113 (3-4) (1994) 397–414.
[24] T. Belytschko, Y. Krongauz, D. Organ, M. Fleming, P. Krysl, Meshless methods: an overview and recent developments, Computer methods in applied mechanics and engineering 139 (1-4) (1996) 3–47.
[25] E. Burman, P. Hansbo, Fictitious domain finite element methods using cut elements: I. a stabilized Lagrange multiplier method, Computer Methods in Applied Mechanics and Engineering 199 (41-44) (2010) 2680–2686.
[26] F. Brezzi, M. Fortin, Mixed and hybrid finite element methods, Vol. 15, Springer Science & Business Media, 2012.

[27] H. J. Barbosa, T. J. Hughes, The finite element method with Lagrange multipliers on the boundary: circumventing the Babuška-Brezzi condition, Computer Methods in Applied Mechanics and Engineering 85 (1) (1991) 109–128.
[28] N. Moës, E. Béchet, M. Tourbier, Imposing Dirichlet boundary conditions in the extended finite element method, International Journal for Numerical Methods in Engineering 67 (12) (2006) 1641–1669.
[29] A. Gerstenberger, W. Wall, An embedded Dirichlet formulation for 3D continua, International Journal for Numerical Methods in Engineering 82 (5) (2010) 537–563.
[30] T. Zhu, S. Atluri, A modified collocation method and a penalty formulation for enforcing the essential boundary conditions in the element free Galerkin method, Computational Mechanics 21 (3) (1998) 211–222.
[31] S. Atluri, T.-L. Zhu, The meshless local Petrov-Galerkin (MLPG) approach for solving problems in elasto-statics, Computational Mechanics 25 (2) (2000) 169–179.
[32] D. Schillinger, M. Ruess, N. Zander, Y. Bazilevs, A. Düster, E. Rank, Small and large deformation analysis with the p-and B-spline versions of the finite cell method, Computational Mechanics 50 (4) (2012) 445–478.
[33] M. Griebel, M. A. Schweitzer, A particle-partition of unity method part V: boundary conditions, in: Geometric analysis and nonlinear partial differential equations, Springer, 2003, pp. 519–542.
[34] A. Embar, J. Dolbow, I. Harari, Imposing Dirichlet boundary conditions with Nitsche's method and spline-based finite elements, International journal for numerical methods in engineering 83 (7) (2010) 877–898.
[35] D. Schillinger, A. Dster, E. Rank, The hp-d-adaptive finite cell method for geometrically nonlinear problems of solid mechanics, International Journal for Numerical Methods in Engineering 89 (9) (2011) 1171–1202.
[36] E. Burman, P. Hansbo, Fictitious domain finite element methods using cut elements: II. a stabilized Nitsche method, Applied Numerical Mathematics 62 (4) (2012) 328–341, nitsche's+ elasticity+ eigen value.
[37] R. Codina, J. Baiges, Approximate imposition of boundary conditions in immersed boundary methods, International Journal for Numerical Methods in Engineering 80 (11) (2009) 1379–1405.
[38] I. Harari, U. Albocher, Spectral investigations of Nitsche's method, Finite Elements in Analysis and Design 145 (2018) 20–31.
[39] J. Dolbow, I. Harari, An efficient finite element method for embedded interface problems, International journal for numerical methods in engineering 78 (2) (2009) 229–252.
[40] A. Apostolatos, R. Schmidt, R. Wüchner, K.-U. Bletzinger, A Nitsche-type formulation and comparison of the most common domain decomposition methods in isogeometric analysis, International Journal for Numerical Methods in Engineering 97 (7) (2014) 473–504, use Nitsche's method to connect non-matching patches.
[41] M. Ruess, D. Schillinger, A. I. Özcan, E. Rank, Weak coupling for isogeometric analysis of non-matching and trimmed multi-patch geometries, Computer Methods in Applied Mechanics and Engineering 269 (2014) 46–71, use Nitsche's method to connect non-matching patches.
[42] P. Hansbo, M. G. Larson, Discontinuous Galerkin methods for incompressible and nearly incompressible elasticity by Nitsche's method, Computer methods in applied mechanics and engineering 191 (17-18) (2002) 1895–1908.
[43] T. Chen, M. Rong, W. Neng, G. Zhongwei, Imposing displacement boundary conditions with Nitsches method in isogeometric analysis (in Chinese), Chinese journal of theoretical and applied mechanics 44 (2) (2012) 371–381.
[44] C. Wei-zang, Method of high-order Lagrange multiplier and generalized variational principles of elasticity with more general forms of functionals, Applied Mathematics and Mechanics 4 (2) (1983) 143–157.
[45] T. H. Pian, K. Sumihara, Rational approach for assumed stress finite elements, International Journal for Numerical Methods in Engineering 20 (9) (1984) 1685–1695.
[46] R. Codina, J. Baiges, Weak imposition of essential boundary conditions in the finite element approximation of elliptic problems with non-matching meshes, International Journal for Numerical Methods in Engineering 104 (7) (2015) 624–654.
[47] Z. Zhang, A. V. Kumar, Immersed boundary modal analysis and forced vibration simulation using step boundary method, Finite Elements in Analysis and Design 126 (2017) 1–12.
[48] I. Y. Kharrik, On approximation of functions that have zero values and derivatives on domain boundary by special functions, Siberian mathematical journal 4 (2) (1963) 408–425.
[49] V. L. Rvachev, T. I. Sheiko, R-functions in boundary value problems in mechanics, Appl. Mech. Rev 48 (4) (1995) 151–188.
[50] V. Shapiro, I. Tsukanov, Implicit functions with guaranteed differential properties, in: Proceedings of the fifth ACM symposium on Solid modeling and applications, ACM, 1999, pp. 258–269.
[51] K. Höllig, C. Apprich, A. Streit, Introduction to the Web-method and its applications, Advances in Computational Mathematics 23 (1-2) (2005) 215–237.
[52] A. V. Kumar, R. Burla, S. Padmanabhan, L. Gu, Finite element analysis using nonconforming mesh, Journal of Computing and Information Science in Engineering 8 (3) (2008) 031005.

[53] R. K. Burla, A. V. Kumar, Implicit boundary method for analysis using uniform B-spline basis and structured grid, International Journal for Numerical Methods in Engineering 76 (13) (2008) 1993–2028.
[54] M. Cortis, W. Coombs, C. Augarde, M. Brown, A. Brennan, S. Robinson, Imposition of essential boundary conditions in the material point method, International Journal for Numerical Methods in Engineering 113 (1) (2018) 130–152.
[55] K. Lu, C. Augarde, W. Coombs, Z. Hu, An implicit boundary finite element method with extension to frictional sliding boundary conditions and elasto-plasticity analyses, Under review.
[56] S. Bertoluzza, M. Ismail, B. Maury, The fat boundary method: semi-discrete scheme and some numerical experiments, Lecture Notes in Computational Science and Engineering 40 (2005) 513–520.
[57] S. Bertoluzza, M. Ismail, B. Maury, Analysis of the fully discrete fat boundary method, Numerische Mathematik 118 (1) (2011) 49–77.
[58] S. L. Campbell, C. D. Meyer, Generalized inverses of linear transformations, Vol. 56, SIAM, 2009.
[59] D. Griffiths, Treatment of skew boundary conditions in finite element analysis, Computers & Structures 36 (6) (1990) 1009–1012.
[60] S. P. Timoshenko, J. N. Goodier, Theory of elasticity, Vol. 3, McGraw-Hill, New York London, 1970.